polymers

MDPI

Article

Role of Bio-Based and Petroleum-Origin Monomers on the Tailoring of Thermoplastic Elastomer (TPE) Properties and Structure as a Matrix for Composites with Plant-Based and Inorganic Fillers

Sandra Paszkiewicz [1,*], Zaida Ortega [2,*], Izabela Irska [1], Konrad Walkowiak [1], Adam Piasecki [3] and Mateusz Barczewski [4]

[1] Faculty of Mechanical Engineering and Mechatronics, West Pomeranian University of Technology in Szczecin, 70-310 Szczecin, Poland; izabela.irska@zut.edu.pl (I.I.); wk42388@zut.edu.pl (K.W.)
[2] Departamento de Ingeniería de Procesos, Universidad de las Palmas de Gran Canaria, C. Juan de Quesada, 30, 35001 Las Palmas de Gran Canaria, Spain
[3] Institute of Materials Engineering, Faculty of Materials Engineering and Technical Physics, Poznan University of Technology, Piotrowo 3, 61-138 Poznan, Poland; adam.piasecki@put.poznan.pl
[4] Institute of Materials Technology, Poznan University of Technology, Piotrowo 3, 61-138 Poznan, Poland; mateusz.barczewski@put.poznan.pl
* Correspondence: sandra.paszkiewicz@zut.edu.pl (S.P.); zaida.ortega@ulpgc.es (Z.O.)

Abstract

This study investigates how natural fillers of different origins and morphologies influence the structural, thermal, rheological, and mechanical properties of thermoplastic elastomers (TPEs). Two series of materials were prepared: one based on a biobased matrix, poly(butylene 2,5-furandicarboxylate)-block-poly(tetramethylene oxide) (PBF-PTMO), and one based on a petroleum-derived matrix, poly(butylene terephthalate)-block-poly(tetramethylene oxide) (PBT-PTMO). Both series incorporated a range of natural modifiers, i.e., lignocellulosic fibers and ground fractions of *Arundo donax* L., cyanobacterial biomass (*Spirulina platensis*), and silica-rich mineral dust originating from volcanic stone quarries. The materials were obtained via melt blending, while the reference matrices (neat block copolymers) were synthesized through melt polycondensation. The chemical structure and limiting viscosity number (LVN) of the neat matrices were confirmed, while differential scanning calorimetry (DSC) provided insight into their morphology and phase composition. Scanning electron microscopy (SEM) was employed to evaluate the morphology and distribution of the modifiers within the polymer matrices. To assess how the fillers influenced processing windows and performance, thermogravimetric analysis (TGA), oscillatory rheological measurements, and tensile testing were performed. The results provide insight into structure–property relationships governing natural filler–TPE interactions and support the development of more sustainable elastomeric composites with tailored performance.

Keywords: furan-based polymers; TPEs; block copolymers; melt polycondensation; natural fillers

Academic Editor: Ana Pilipović

Received: 16 December 2025
Revised: 16 February 2026
Accepted: 17 February 2026
Published: 19 February 2026

1. Introduction

Thermoplastic elastomers (TPEs) represent an important class of advanced polymer materials that combine the elastic behavior of rubbers with the processability of thermoplastics [1,2]. Their unique performance originates from phase-separated microstructures,

in which hard and soft domains coexist, providing a balance between mechanical strength and flexibility. Among TPEs, segmented block copolymers based on polyester structures have attracted particular attention due to their tunable morphology and broad application potential in the automotive, consumer goods, and biomedical fields [3–7]. Due to the possibility of tailoring unique properties arising from their structure, the application range depends only on the specified industrial needs. The final properties of the copolymer are influenced by the synthesis method and the control over the molecular weight and distribution of the segments within the final structure of the copolymer, as well as by the ratio between the soft and the hard segments [8,9]. In polyester-based segmented block copolymers, phase separation is predominantly driven by crystallization processes [10]. Among them, multiblock poly(ether–ester)s (PEEs) comprising poly(butylene terephthalate) (PBT) as the rigid domains and poly(tetramethylene oxide) (PTMO) as the flexible segments have been the subject of extensive research [3,11–14]. Owing to their outstanding mechanical performance, particularly the combination of high strength and elasticity over a broad temperature range, these materials are of considerable technological interest. Notably, PBT-block-PTMO copolymers have already been commercialized under trade names such as Elitel™, Arnitel®, and Hytrel® (DSM). However, recently, furan-based polyesters that are derived from plant-sourced 2,5-furandicarboxylic acid (FDCA), particularly poly(butylene 2,5-furan dicarboxylate) (PBF), have emerged as promising candidates to replace conventional PBT rigid segments [15–18]. When copolymerized with renewable poly(tetramethylene oxide) (PTMO), they enable the development of fully biobased thermoplastic poly(ether–ester)s (TPEEs) [19–21]. The increasing research interest in furan polyesters is driven mainly by the global pursuit of renewable feedstocks, primarily from green biomass [22–25], to mitigate the depletion of fossil resources, reduce energy consumption and greenhouse gas emissions during monomer and polymer production, and promote the valorization of agricultural by-products. Furthermore, studies on the recyclability and closed-loop applications of these polymers highlight their additional environmental benefits [26–28]. Comparative analyses indicate strong structural and property analogies between furan- and terephthalate-based polyesters [17]. However, for thermoplastic elastomers, material performance is dictated by phase separation induced through the crystallization of the rigid segments. In bio-based analogs, the crystallization behavior is strongly influenced by the intrinsic structural features of the furan ring, including its non-linear linkages with aliphatic chains and its higher polarity relative to the benzene ring of terephthalates [15,29–34].

Despite their potential, these copolymers still face challenges. Phase separation between hard and soft segments may lead to heterogeneous properties, while composition and processing strongly influence mechanical performance, sometimes resulting in inconsistencies [5,35]. Differences in thermal behavior between PBF or PBT and PTMO further complicate processing, increasing costs and limiting scalability [36]. In composites, inefficient load transfer to fillers can reduce mechanical strength [37]. Nevertheless, the ability to tailor formulations for targeted applications makes these materials highly promising [38,39]. Therefore, incorporating PBF or PBT-PTMO copolymers as the polymer matrix in composite materials offers a promising path to enhance the mechanical, thermal, and functional properties of various applications. The unique characteristics of these copolymers make them suitable composite matrices for various fillers, including nanoparticles. For instance, the introduction of fillers, such as carbon nanotubes (CNTs) or graphene, into PBT-PTMO and PTT-PTMO copolymers has been shown to enhance their mechanical and thermal properties. Some studies have shown that adding CNTs to PBT-PTMO copolymers improves tensile strength and thermal conductivity, making these materials more suitable for high-performance applications [40,41].

As the demand for sustainable materials increases, furan-based copolymers can be designed to incorporate renewable resources or biodegradable components. This aspect aligns with the growing interest in developing environmentally friendly materials that reduce reliance on fossil fuels and minimize environmental impact [35,42]. In this sense, this research proposed the use of several natural fillers of different natures: lignocellulose (fibers and ground material from *Arundo donax* L.), cyanobacteria (*Spirulina platensis*), and mineral dust (based on silica, derived from quarries of volcanic stone) to determine how the nature and morphological features (size and shape, fibrous vs. particle) affect the final properties of the petroleum- and bio-based TPEs. These block copolymers have not yet been studied in depth for the production of composites. In particular, no previous research on the use of natural fillers, as those proposed in this study, is found in the literature. Such fillers can provide not only interesting advanced properties but also a potential reduction in costs due to the low cost of the proposed materials. Consequently, the study evaluates the feasibility of bio-based TPEs as sustainable alternatives without compromising material functionality, since biomass- or plant-derived materials are often regarded as carbon neutral, as the CO_2 released during their use is offset by the CO_2 absorbed by plants during growth [43,44].

The incorporation of lignocellulosic fillers into furan-based and petroleum-based block copolymers presents a promising approach to enhance the mechanical, thermal, and environmental properties of these materials. Lignocellulosic fillers, derived from plant biomass, offer several advantages, including renewability, biodegradability, and cost-effectiveness, making them an attractive option for sustainable composite materials. The integration of Spirulina, a type of cyanobacteria recognized for its bioactive compounds, into these copolymers offers an innovative approach to developing sustainable composite materials that enhance the properties of the polymer matrices.

Finally, the use of silica-based fillers (such as stone dust in this case) is a promising strategy to improve the mechanical, thermal, and functional properties of TPEs. Silica fillers are well known for their reinforcing capability and can significantly enhance the overall performance of polymer composites, making them suitable for a wide range of applications that require high strength and durability. In addition to mechanical reinforcement, mineral fillers such as silica can improve the thermal stability of the materials and increase their thermal conductivity, thereby facilitating heat dissipation and improving overall thermal performance.

This study aims to evaluate how natural fillers of different origins, i.e., lignocellulosic materials (fibers and ground fractions of *Arundo donax* L.), cyanobacterial biomass (*Spirulina platensis*), and silica-rich mineral dust derived from volcanic stone quarries, affect the final properties of both bio-based and petroleum-based thermoplastic elastomers. The research focuses on elucidating the role of filler nature and morphology (size, shape, and fibrous versus particulate character) at a constant filler loading of 5 wt.%, selected to ensure good processability while enabling a direct comparison of filler–matrix interactions and reinforcement effects across different filler types. The chemical structure and limiting viscosity number (LVN) of the neat polymer matrices were confirmed, while differential scanning calorimetry (DSC) was used to investigate morphology and phase structure. SEM analysis was also performed to determine the influence of the different fillers on the morphology of the final composite and to link the microstructure with the composite's properties. To assess processing-temperature constraints and application potential arising from filler-induced changes, thermogravimetric analysis (TGA), rheological measurements, and tensile testing were performed on both series of materials.

2. Materials and Methods

2.1. Materials

2.1.1. Reagents, Synthesis of PBF-PTMO and PBT-PTMO

The PBF-PTMO and PBT-PTMO copolymers, which constitute the polymer matrices for two series of composites, were prepared by a polymerization process that can be divided into two main stages: transesterification and polycondensation. During transesterification, dimethyl 2,5-furandicarboxylate (DMFDC, 99.9%, Henan Coreychem Co., Ltd., Zhengzhou, China) for PBF-PTMO and dimethyl terephthalate (DMT, Sigma-Aldrich, St. Louis, MO, USA) for PBT-PTMO reacted with butylene glycol (BD, 99%, Alfa Aesar, ThermoFisher (Kandel) GmbH, Kandel, Germany). The reaction proceeded at 160–185 °C under atmospheric pressure with titanium butoxide ($Ti(OBu)_4$, TBT, 97%, Merck, Darmstadt, Germany) as the catalyst for up to two hours. During this step, methanol, the by-product, was continuously distilled, and completion was confirmed when ~90% of the theoretical amount was collected. Before polycondensation, poly(tetramethylene oxide) (PTMO, Mn = 1000 g/mol, 99%, BASF, Ludwigshafen, Germany), a thermal stabilizer (Irganox 1010, Ciba Geigy, Basel, Switzerland), and a second dose of TBT were introduced. The mixture was then heated to 240 °C, and a vacuum (25 Pa) was applied for up to 1.5 h to remove excess BD. Reaction progress was monitored via stirrer torque, an indicator of melt viscosity, and the process was terminated once the target viscosity and, thus, molecular weight were achieved. The polymer was extruded through the heated nozzle under nitrogen into a water bath, yielding about 70%. The final copolyesters contained ~45 wt.% rigid segments (PBF or PBT) and ~55 wt.% soft PTMO segments. The limiting viscosity number (LVN) of PBF-PTMO was 1.092 dL/g, and the LVN of PBT-PTMO was 1.131 dL/g.

2.1.2. Characteristics of Fillers (Modifiers)

Four different fillers were added at 5 wt.% to the synthesized copolymers. Fillers with different natures and properties were selected to understand the potential changes in the matrix resulting from their composition and properties. In particular, mineral dust obtained as waste from ignimbrite quarries was used. This material has a very fine granulometry and is mostly composed of silica and alumina (62.5% SiO_2 and 17.8% Al_2O_3), with lower amounts of other oxides [45]. This material has superior thermal stability (with no degradation under either air or nitrogen atmospheres up to 900 °C), a density of approximately 2.45 g/cm^3, and a particle size under 50 µm. In addition, biomass derived from the cyanobacterium Spirulina platensis was used as a filler. Spirulina shows low thermal stability, with a lower limit temperature around 140 °C but a high content of antioxidant compounds (over 900 mg TPC/100 g biomass) and a free radical scavenging potential close to 35%, which might lead to a higher stability of the final material under oxidizing conditions. Finally, two materials derived from *Arundo donax* L. (giant reed) were also assessed; one of them (shredded) was prepared by simply grinding the aerial parts of the reed culms, while the other one (fibers) was obtained after a chemo-mechanical procedure on those culms. Both methods, along with their complete characterization, can be found elsewhere [46,47]. In summary, fibers are more thermally stable than shredded material and also exhibit a higher mechanical performance, although the shredded material shows a higher content of antioxidants, which might be beneficial for increasing the stability of the composite. Composites with a constant share of the fillers were named according to the filler they contained, namely "Ign" for ignimbrite dust, "Sp" for Spirulina, "RF" for reed fibers, and "Reed" for shredded reed added to the polymeric matrix designation. Table 1 summarizes the main geometrical features of the four materials used as fillers.

Table 1. Summary of geometrical features of the fillers.

Filler	Shape	Diameter (Length)	Reference
Ignimbrite dust (Ign)	Particles	15 µm	[45]
Spirulina (Sp)	Particles	<50 µm	[48]
Arundo fibers (RF)	Fibers	156.5 ± 73.5 µm (1.5 ± 0.5 mm)	[47] [49]
Arundo (Reed)	Particles	370.3 ± 133.0 µm	[47]

2.1.3. Preparation of Two Series of Composites and Sample Preparation

Two series of composites were prepared based on PBF-PTMO or PBT-PTMO matrices and several natural fillers of different origins: lignocellulose (fibers and ground material from *Arundo donax* L.), cyanobacteria (*Spirulina platensis*), and mineral dust (silica-based, derived from volcanic stone quarries), with a fixed filler content of 5 wt.% (Figure 1). Before melt mixing, both the polymer granules and fillers were dried in a laboratory vacuum oven (Binder ED115, Tuttlingen, Germany) at 60 °C for 24 h. Melt mixing was carried out using a Brabender mixer (Plasti-Corder Model PL2100, Brabender GmbH & Co. KG., Duisburg, Germany) at 185 °C for PBF-based composites and 205 °C for PBT-PTMO-based ones, with a mixing time of 5 min for all formulations. The obtained composites were subsequently compression-molded at 185 °C (PBF-PTMO) or 205 °C (PBT-PTMO) for 2 min under 1 MPa using a laboratory hydraulic press (P 200 E, Dr. Collin GmbH, Maitenbeth, Germany) to obtain specimens for further analyses. Plates with dimensions of 100 mm × 100 mm × 4 mm were prepared. From these plates, test specimens for mechanical characterization (type A3) were cut using a Collin P200P press equipped with a standardized die according to PN-EN 60811-501 [50]. Specimens were prepared at room temperature under 2 MPa pressure for 30 s.

Figure 1. Photography of the series of composites, from left: PBF-PTMO, PBF-PTMO + 5% Reed, PBF-PTMO + 5% RF, PBF-PTMO + 5% Ign, PBF-PTMO + 5% Sp, and second series: PBT-PTMO, PBT-PTMO + 5% Reed, PBT-PTMO + 5% RF, PBT-PTMO + 5% Ign dust, PBT-PTMO + 5% Sp.

2.2. Characterization Methods

The molecular structure of the prepared PBF-PTMO and PBT-PTMO, which constitute the composite matrices, was determined using ^{1}H NMR spectroscopy. Prior to analysis, all samples underwent continuous Soxhlet extraction with methanol to remove residual monomers and potential low-molecular-weight degradation products. Proton nuclear

magnetic resonance (^{1}H NMR) spectra were acquired at room temperature using a Bruker spectrometer operating at 400 MHz. The samples were prepared in chloroform-d ($CDCl_3$) at a concentration of 10 mg/mL, with tetramethylsilane (TMS) serving as the internal chemical shift reference.

The limiting viscosity number (LVN) of the synthesized copolymers was determined using a capillary Ubbelohde viscometer (type I_c, K = 0.03294). The mixture of phenol/1,1,2,2-tetrachloroethane (60/40 by weight) was used as the solvent. The polymer solution had a concentration of 0.5 g/dL. The measurement was carried out at 30 °C.

Attenuated total reflectance–Fourier transform infrared (ATR-FTIR) spectra were collected using a PerkinElmer Two spectrophotometer (PerkinElmer, Waltham, MA, USA). Each spectrum was acquired over the 4000–400 cm^{-1} range with a resolution of 4 cm^{-1} and averaged from 64 scans.

Scanning electron microscopy (SEM) was performed using the Tescan MIRA3 microscope. The measurements were conducted with an accelerated voltage of 12 kV and magnifications of 100×, 200×, 1000×, and 2000×. A thin carbon coating (∼20 nm) was deposited on the samples using the Jeol JEE 4B vacuum evaporator.

The characteristic phase transition temperatures, including the glass transition (T_g), melting (T_m), and crystallization (T_c) temperatures, were analyzed using a DSC 204 F1 Phoenix® calorimeter (Netzsch, Selb, Germany) under a nitrogen atmosphere. Measurements were performed in a heating–cooling–heating cycle at a rate of 10 °C/min over the temperature range of −85 to 250 °C for both PBF-PTMO and PBT-PTMO. T_g and T_m values were determined from the second heating run, with T_g obtained by the midpoint method, and the change in specific heat capacity (ΔC_p) calculated as the vertical distance between extrapolated baselines at T_g. Crystallization and melting temperatures were identified from the maxima of the exothermic and endothermic peaks, respectively. The enthalpies of fusion (ΔH_m) and crystallization (ΔH_c) were obtained by integrating the areas under the corresponding peaks of the DSC thermograms.

Thermal stability was evaluated under a nitrogen atmosphere at a flow rate of 10 mL/min. Measurements were carried out from 30 to 700 °C with approximately 15 mg of material placed in alumina crucibles and analyzed on a PerkinElmer TGA 4000 instrument (PerkinElmer, Waltham, MA, USA).

The static mechanical properties were measured using an Autograph AG-X plus universal testing machine (Shimadzu, Kyoto, Japan) equipped with a 1 kN Shimadzu load cell, operated at a constant crosshead speed of 5 mm/min. Measurements were performed at room temperature on the dumbbell-shaped samples with a grip distance of 20 mm. According to the PN-EN ISO 527 standard [51], the Young's modulus, tensile strength at yield (σ_y), strain at yield (ε_y), tensile strength at break (σ_b), and strain at break (ε_b) of PBF and its block copolymers were determined. The reported values are the means of 5 measurements. The toughness, defined as the energy absorbed until fracture, was evaluated by calculating the area under the tensile stress–strain curve. A minimum of five specimens were tested for each material [52]. In addition, the Shore D hardness (H) was measured using a Zwick 3100 Shore D tester (Zwick GmbH, Ulm, Germany). Each reported value is the mean of 10 independent measurements.

Rheological analysis was performed using small-angle oscillatory rheometry (SAOS) with an Anton Paar MCR 301 rotational rheometer in a plate–plate configuration, with a diameter of 25 mm and a gap of 1.5 mm. Before frequency-sweep experiments, all series were tested in an amplitude sweep test, during which the linear viscoelastic range (LVE) was assessed. Frequency-sweep experiments were conducted at 190 °C for PBF-PTMO composites and 210 °C for PBT-PTMO series in the angular frequency range of 0.2 to 500 rad/s with a strain of 0.5%.

3. Results and Discussion

3.1. ^{1}H NMR of the Polymer Matrix

NMR spectroscopy was used to investigate the chemical structure of the synthesized polymer matrices. The ^{1}H NMR spectra of PBF-PTMO and PBT-PTMO are presented in Figure 2, and the theoretical chemical structures, together with those estimated from ^{1}H NMR analysis, are summarized in Table 2. Both copolymer matrices exhibit sharp signals at chemical shifts consistent with expected copolymer structures. The furan ring protons are observed at 7.21 ppm (peak a), in agreement with previously reported values for PBF-based systems [53,54]. Signals at 4.39 ppm (peak b) and 1.91 ppm (peak c) are associated with the methylene groups originating from butylene glycol. Successful incorporation of PTMO into the chemical structure is confirmed by the presence of signals at 4.35 ppm (peak d), 1.83 ppm (peak e), 3.41 ppm (peak g), and 1.61 ppm (peak f), which is consistent with the reported chemical shifts for PTMO units in PBF-b-PTMG copolymers by Kwiatkowska et al. [17]. In the PBT-PTMO ^{1}H NMR spectra, the four aromatic protons of the terephthalic ring (peak h) appear as a singlet at 8.10 ppm. Two signals at 4.46 ppm (peak i) and 1.99 ppm (peak j) arise from the methylene groups of butylene glycol. These observations are consistent with previously reported ^{1}H NMR spectra of PBT [55,56]. As in the case of PBF-PTMO, successful incorporation of PTMO into the chemical structure can be observed. The signals associated with the PTMO unit are observed at 4.39 ppm (peak k), 3.59 ppm (peak n), 1.84 ppm (peak l), and 1.67 ppm (peak m). The weight fractions of the flexible segments were calculated using the peak areas of the furan ring (peak a) for PBF-PTMO, the terephthalate ring (peak h) for PBT-PTMO, and, for both polymer matrices, peaks f and m originating from PTMO, according to Equation (1):

$$W_F = \frac{\left(\frac{I_F}{y}\right) \times M_{WF}}{\left(\frac{I_F}{y}\right) \times M_{WF} + \left(\frac{I_R}{x}\right) \times M_{WR}} \quad (1)$$

where I_R and I_F are the peak areas of the signals assigned to the rigid and flexible segments, respectively, x and y are the numbers of protons contributing to these signals, and M_{WR} and M_{WF} are the molecular weights of the repeating units of the rigid and flexible segments, respectively. The difference between the theoretical and calculated weight fraction is approximately 3.7% for PBF-PTMO and 1.5% for PBT-PTMO. This discrepancy may arise from the introduction of additional PTMO due to losses during dosing of the viscous substrate and distillation of the reaction substrate under reduced pressure [57,58].

Table 2. Polymer matrix composition.

Samples	Feed Molar Ratio (mol%)		^{1}H NMR (mol%)	
	PBF/PBT	PTMO	PBF/PBT	PTMO
PBF-PTMO	1.65	0.60	41.3	58.7
PBT-PTMO	1.90	0.56	43.5	56.5

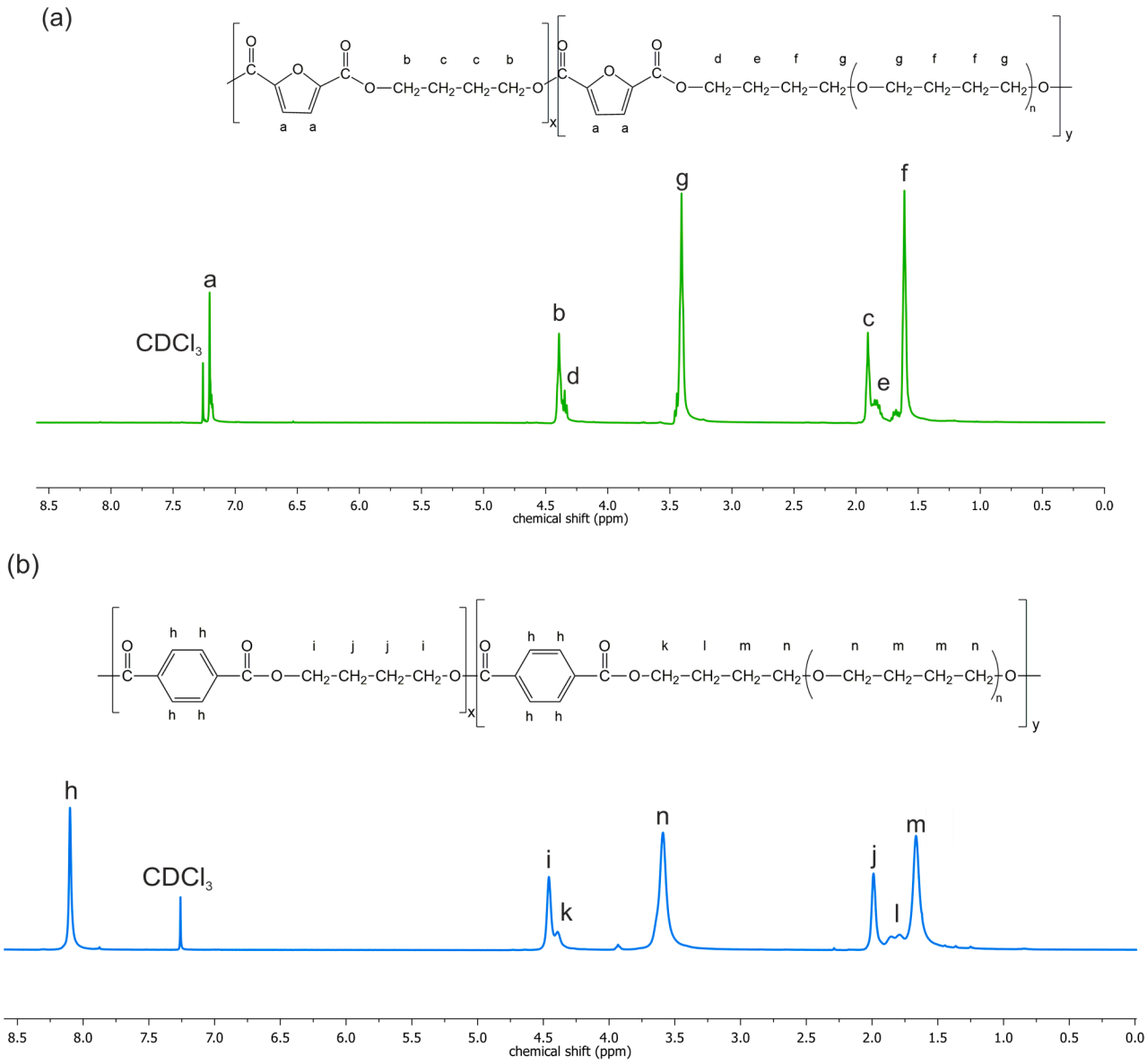

Figure 2. The ^{1}H NMR spectra of PBF-PTMO (**a**) and PBT-PTMO (**b**).

3.2. FTIR

Fourier-transform infrared spectroscopy (FTIR) was employed to characterize the chemical structure and confirm the successful synthesis of both series of TPE-based composites. The FTIR spectra typically display characteristic peaks corresponding to the ether linkages of PTMO and the ester groups of PBT or PBF, providing insights into the copolymers' molecular structure [5,59–61] (Figure 3). A prominent peak at 1712 cm^{-1} corresponds to the C=O stretching vibration of ester groups, accompanied by bands at approximately 1267 and 1100 cm^{-1} assigned to C–O and C–O–C stretching. The absorption band at 1574–1577 cm^{-1} originates from C=C stretching in the aromatic ring. Bands related to asymmetric and symmetric stretching of –CH_2– groups from the butylene units of PBF or PBT and from PTMO segments appear at 2854–2860 and 2940–2963 cm^{-1}. A weak absorption near 2795–2798 cm^{-1} is attributed to symmetric C–H stretching of alkyl groups [17,62]. For PBT-PTMO copolymers, a strong band at ~726 cm^{-1} is associated with out-of-plane C–H deformation of the aromatic ring and the alkane backbone [63,64]. In contrast, PBF-PTMO copolymers exhibit signals characteristic of the furan ring: two weak peaks at 3118 and 3140 cm^{-1} assigned to C–H stretching modes, and additional vibrations at 964, 822, and

763 cm^{-1} typical of 2,5-disubstituted furans. Notably, the band at 763 cm^{-1} is bimodal due to overlapping contributions from C–H vibrations of the alkane backbone [65]. Unfortunately, the FTIR analysis reveals only the typical bands for the matrices, with no significant modification due to filler incorporation, neither in PBF-PTMO nor in PBT-PTMO-based compositions. This evidence shows the lack of chemical interactions between the fillers and the matrices, which is related to the low filler content (5 wt.%), while maintaining their good dispersion within the bulk material, which is crucial for the performance of the final composite.

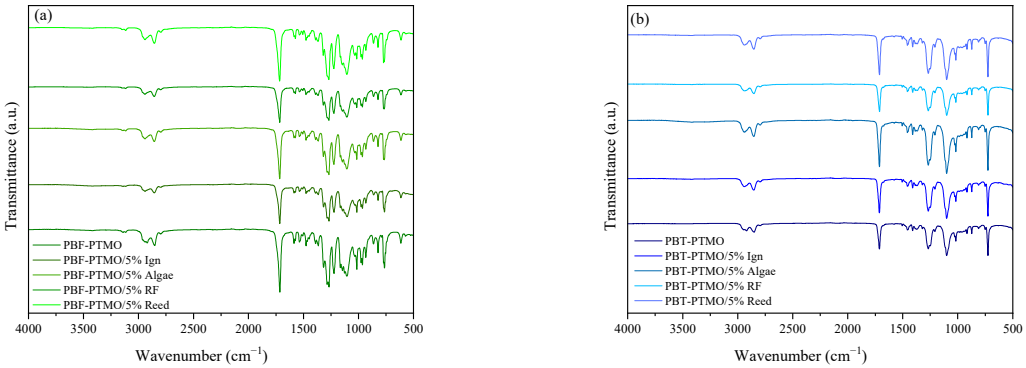

Figure 3. FTIR spectra for the series of composites based on PBF-PTMO (**a**) and for the series of composites based on PBT-PTMO (**b**).

3.3. SEM

Scanning electron microscopy was used to visualize the microstructure of the polymer matrices and incorporated modifiers, assess the distribution and interactions of fibers/particles with polymeric matrices, detect structural imperfections such as voids and cracks, and describe the shape and surface features of the fillers. SEM images were acquired at four magnifications (×200, ×500, ×1k, and ×2k) (Figure 4) to assess the fillers' dispersion and the overall morphological features of the samples, as well as to examine interfacial interactions and characteristic microstructural features at higher magnifications.

SEM images of PBF-PTMO and PBT-PTMO showed very similar morphologies, with both exhibiting a homogeneous two-phase structure typical of thermoplastic elastomers. No pronounced phase separation or distinct domain boundaries were observed at the investigated magnifications, indicating good compatibility between the rigid polyester segments and the flexible, PTMO-rich segments, which is in alignment with previous reports on segmented poly(ester–ether) copolymers [66–68]. Minor surface irregularities were attributed to fracture-induced features rather than intrinsic morphological differences.

SEM analysis revealed distinct differences in ignimbrite dispersion between the two copolymer matrices. In PBF-PTMO containing 5 wt.% Ign, the filler was predominantly present as localized clusters, with occasional isolated particles, resulting in a sponge-like microstructure that may indicate partial filler–matrix incompatibility or preferential localization within the softer domains. In contrast, PBT-PTMO exhibited a more uniform distribution of Ign, with mainly individual particle inclusions observed at all magnifications and no evidence of pronounced agglomeration, suggesting better dispersion and interfacial stabilization within this matrix. The better dispersion of the particles within the PBT-PTMO matrix is in line with the higher mechanical properties observed for this composite compared to that based on PBF-PTMO. A similar correlation between uniform filler dispersion, strong interfacial interactions, and improved mechanical integrity has been reported by Zhang et al. [69], who demonstrated that the absence of particle aggregation and pull-out on cryo-fractured surfaces is indicative of effective filler–matrix adhesion in elastomeric systems.

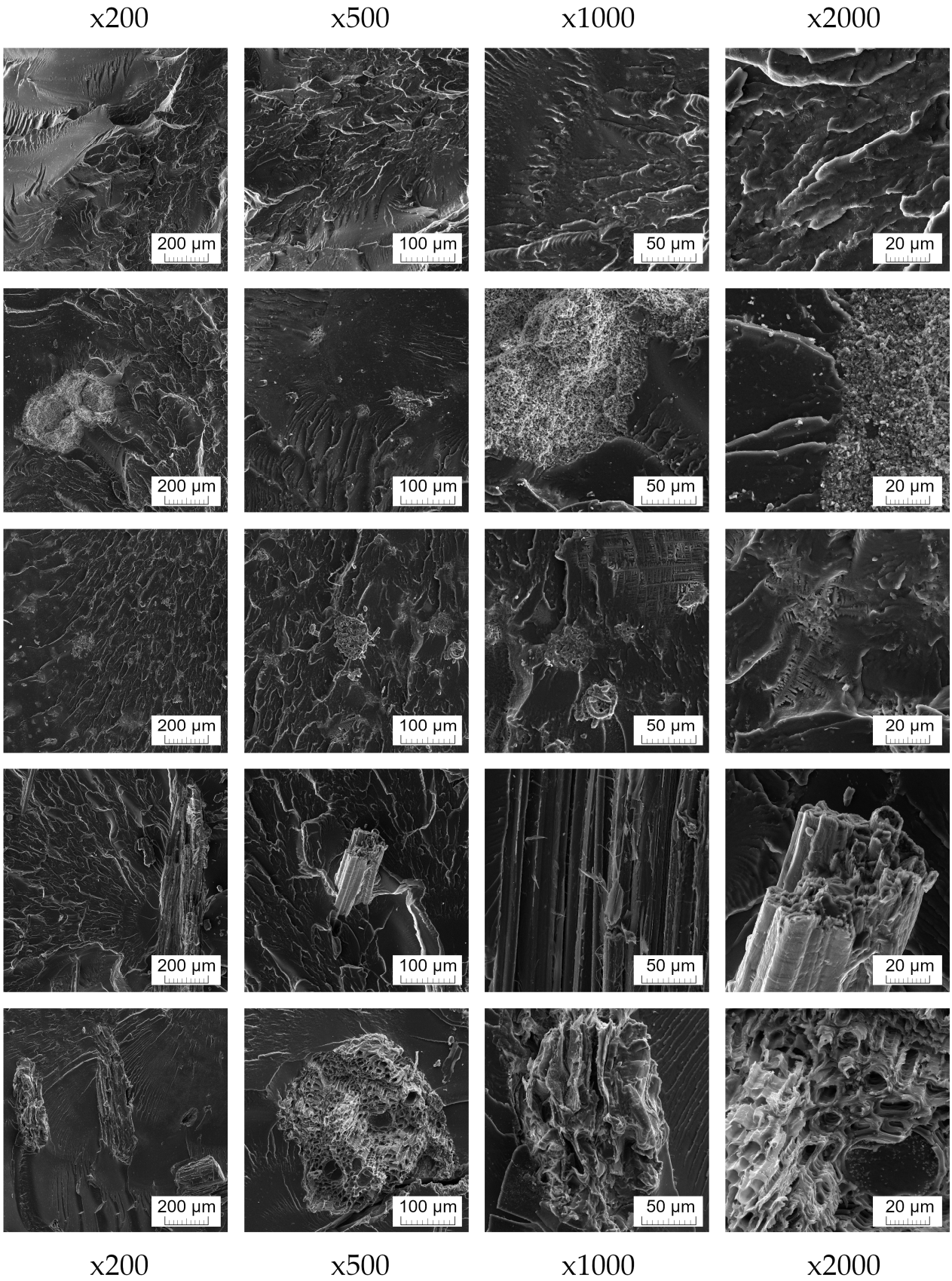

Figure 4. *Cont.*

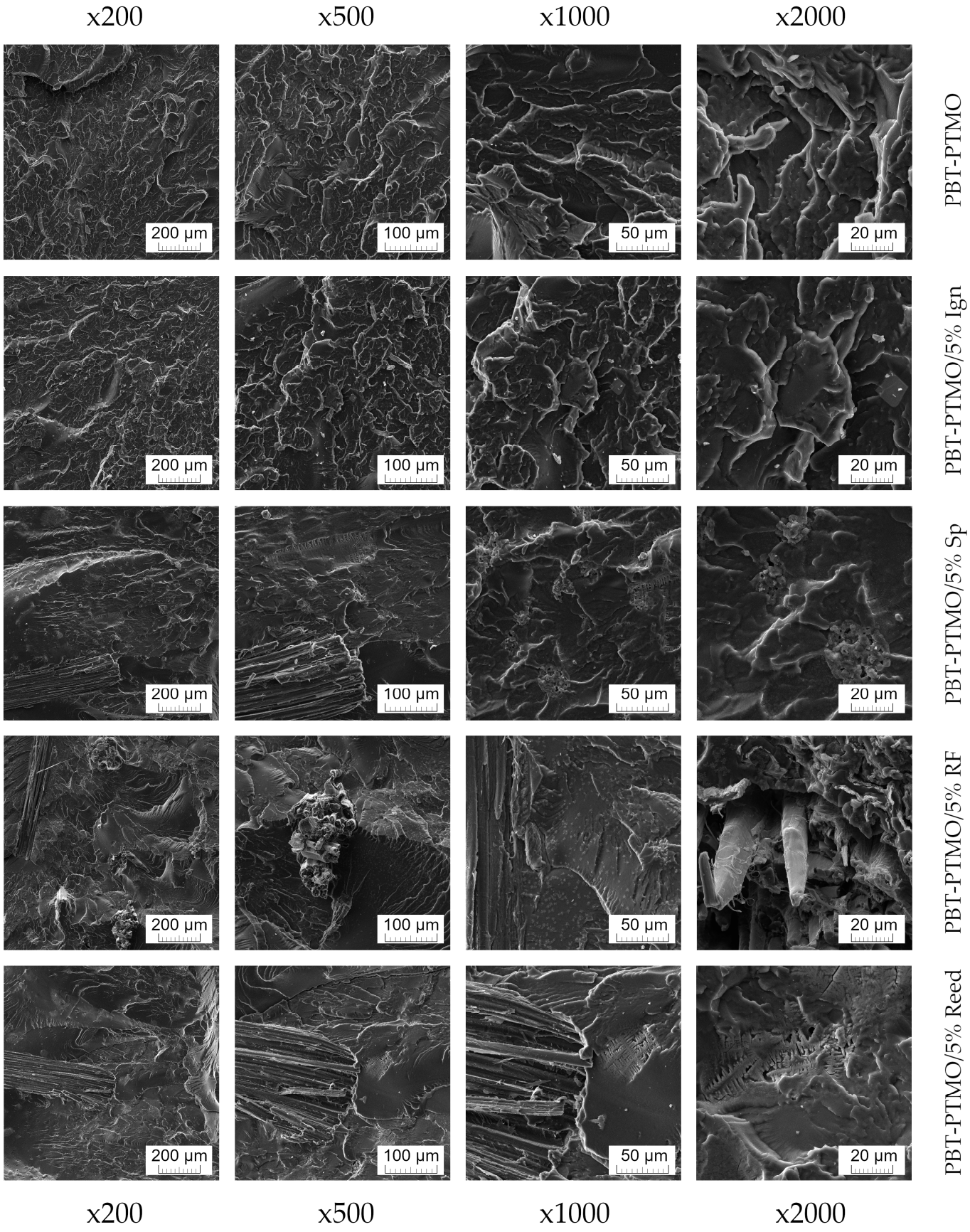

Figure 4. SEM micrographs for both series of composites at selected magnifications (×200, ×500, ×1k, ×2k).

The incorporation of *Spirulina platensis* resulted in the formation of distinctive, non-uniform inclusions within both PBF-PTMO and PBT-PTMO copolymers' matrices. In addition to these irregular features, well-defined crystalline structures with a dendritic morphology were observed. Although small agglomerates were present, the Spirulina particles were generally well dispersed throughout both polymer matrices, indicating relatively homogeneous distribution despite the complex filler morphology.

For composites containing reed fibers (RFs) and shredded reed, SEM images revealed the characteristic fibrous morphology of the natural fillers, accompanied by the presence of crystalline structures similar to those observed for Spirulina-filled systems. As Nie et al. discussed for random poly(p-dioxanone-co-butylene-co-succinate) copolyesters [70], the development of a dendritic crystalline structure is affected simultaneously by various factors, such as amorphous domain content, crystallization temperature, and random chain structure. In this case, it is influenced by the presence of fillers that can cause simultaneous nucleation effects as well as selective hydrolytic degradation due to residual water. The complex interaction of all these effects, along with the simultaneous change in the thermal diffusivity of the composite melt, results in a differentiated interaction forced by intensive cooling, which affects the distance in the interlamellar region of copolymers, driving the breakdown of faceted crystals into dendritic morphologies [70]. However, the correlation between degradation-induced chain scission and changes in crystalline morphology remains a hypothesis in such complex systems, and further research is required to fully understand it. Notably, in PBT-PTMO reinforced with reed fibers, distinct dendritic crystalline domains were observed, which may reflect localized crystallization phenomena induced by processing conditions and filler–matrix interactions. Similar to observations reported for elastomeric systems with limited thermodynamic compatibility, insufficient interfacial interactions may promote local phase separation and filler exposure at fracture surfaces, thereby influencing crystalline organization and morphology development [71]. This comparison highlights the importance of interfacial compatibility in suppressing delamination and enabling more homogeneous microstructural evolution, even in the absence of specific chemical coordination mechanisms.

3.4. DSC Analysis

Using differential scanning calorimetry (DSC), the synthesized matrices and their composites were examined to determine how the incorporation of 5 wt.% of various fillers influenced their thermal behavior. The two multiblock copolymer systems exhibit notable differences in their thermal characteristics, as reflected in the phase transition temperatures detected during cooling and the subsequent heating cycle (second heating scan) in the DSC analysis. These changes, summarized in Figure 5 and Table 3, highlight the influence of monomer origin (renewable or non-renewable), composition, and filler addition on crystallization and melting behavior.

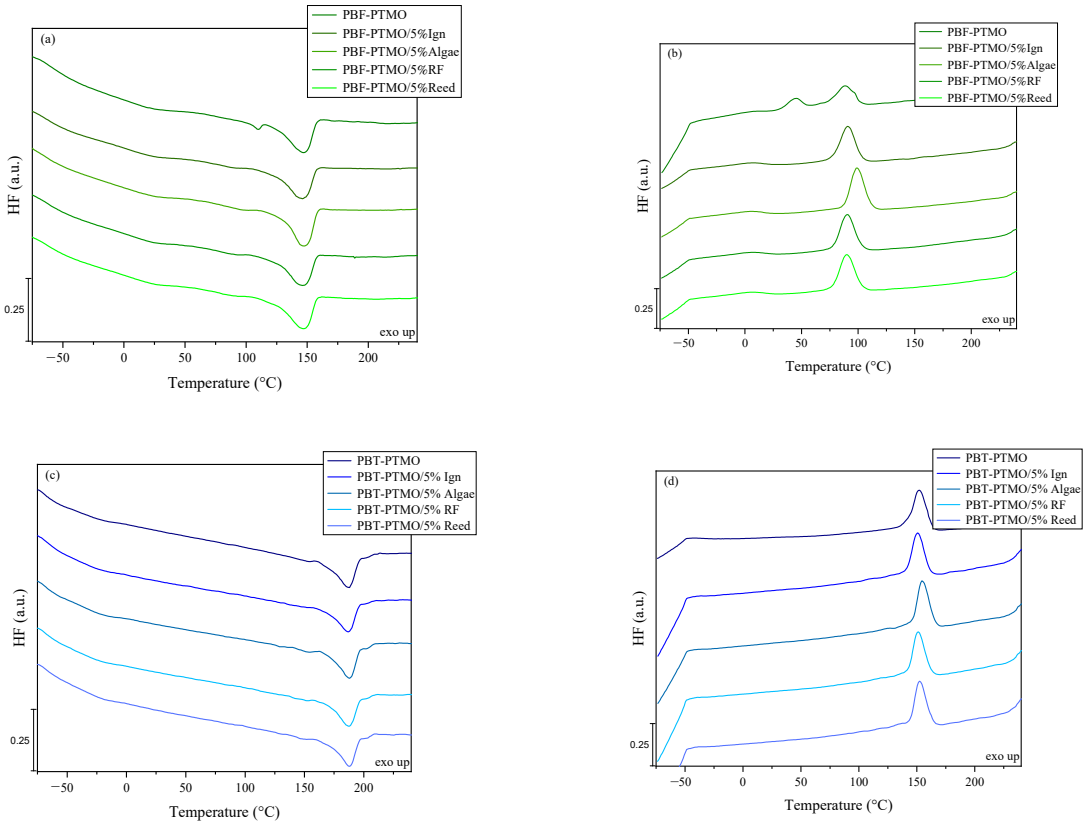

Figure 5. DSC curves recorded during second heating (**a**) and cooling (**b**) for the series of composites based on PBF-PTMO and during second heating (**c**) and cooling (**d**) for the series of composites based on PBT-PTMO.

Table 3. Thermal properties of the obtained materials.

Sample	T_{gF} [°C]	ΔC_{pF} [J/g·K]	T_{gR} [°C]	ΔC_{pR} [J/g·K]	T_m [°C]	ΔH_m [J/g]	T_c [°C]	ΔH_c [J/g]
SERIES I								
PBF-PTMO	−59.9	0.102	27.6	0.061	109.7; 147.4	22.7	44.3; 87.9	22.6
PBF-PTMO/5% Ign	−60.8	0.111	27.4	0.038	146.1	24.9	91.0	24.3
PBF-PTMO/5% Sp	−60.3	0.024	26.4	0.023	146.9	26.9	99.2	26.7
PBF-PTMO/5% RF	−60.6	0.078	27.1	0.011	146.1	27.7	91.2	27.2
PBF-PTMO/5% Reed	−60.1	0.244	27.3	0.010	147.6	25.9	90.4	25.5
SERIES II								
PBT-PTMO	−66.2	0.179	47.2	0.017	186.5	36.6	151.7	35.9
PBT-PTMO/5% Ign	−65.0	0.123	48.7	0.019	187.0	30.3	150.3	30.2
PBT-PTMO/5% Sp	−65.1	0.099	48.0	0.087	187.6	33.5	154.5	33.2
PBT-PTMO/5% RF	−65.8	0.103	47.2	0.010	187.1	30.3	151.0	31.4
PBT-PTMO/5% Reed	−65.4	0.092	46.4	0.009	187.8	27.9	152.3	27.1

Tg_F, glass transition temperature of flexible segment and corresponding ΔCp_F, change in heat capacity; Tg_R, glass transition temperature of rigid segment and corresponding ΔCp_R, change of heat capacity; T_m, ΔH_m, melting temperature and the corresponding enthalpy of melting; T_c, ΔH_c, crystallization temperature and the corresponding enthalpy of crystallization.

In the PBF-PTMO block copolymer series, the most pronounced differences between the unmodified matrix and its modified counterparts arise from melting and crystallization behavior. Generally, the rigid, aromatic furan segments act as initial nuclei and are responsible for copolymer crystallization, while the linear, soft segments are associated with the amorphous region of the materials and influence the glass transition [58,72–75]. The neat

PBF-PTMO exhibits two distinct melting and crystallization peaks on DSC curves, whereas the incorporation of 5 wt.% of each modifier eliminates the lower-temperature peak, indicating suppression of the less stable crystalline structure development during crystallization from the melt. The addition of modifiers does not shift the glass transition temperature of the soft PTMO segment. However, the corresponding changes in heat capacity increment (ΔC_p) are slightly reduced for the composites containing cyanobacterial biomass (Sp) and reed fibers (RFs). The glass transition temperatures of the rigid segments (T_{gR}) remain comparable within the series. Notably, T_{gR} values are lower than those reported for neat PBF (ca. 39–40 °C [76,77]), which supports partial miscibility between the hard and soft phases rich in PBF or rich in PTMO [78]. This trend is consistent with earlier observations for furan-based copolymers reported in the literature [17,57,79]. The incorporation of modifiers does not significantly shift melting or crystallization temperatures. Nevertheless, a slight increase in melting and crystallization enthalpies is observed, most prominently for RF-filled samples, suggesting a nucleating or crystallization-promoting effect. Similarly, Deng et al. [80] observed negligible changes in T_g and T_m values for PBF-based copolymers after extrusion and injection molding, with or without fiber incorporation. These observations are also consistent with our previous results obtained for copoly(ester–ether)s based on poly(trimethylene 2,5-furandicarboxylate) (PTF-PTMO), although in that study, a lower amount of filler/modifier (1 wt.%) was incorporated, wherein the nanocomposites were prepared via an in situ approach [81]. In that system, the melting temperatures (T_m) of all materials did not differ significantly upon the addition of carbon or mineral nanofillers. The incorporation of nanoparticles increased crystallinity (X_c) but primarily influenced the glass transitions of the rigid and flexible segments, chain folding, and, consequently, the cold- and melt-crystallization behavior. Notably, only carbon nanofillers acted as effective nucleating agents, as crystallization from the melt was observed exclusively for the PTF-PTMO/1% graphene nanoplatelet (GNP) composite. In contrast, the addition of other nanofillers, particularly mineral-originated ones, such as halloysite nanotubes (HNTs) and organoclay (C20A), predominantly affected chain-folding processes rather than acting as nucleating agents.

In this study, the series based on the PBT-PTMO copolymer shows an even weaker influence of 5 wt.% filler addition. No measurable changes in the glass transition temperatures of either the rigid or flexible segments are detected. As expected, T_{gR} values are higher than those of the PBF-based series due to the intrinsically higher glass transition temperature of neat PBT (37–52 °C [82,83]). The melting temperature (T_m) remains unaffected mainly upon filler presence, displaying only a slight upward shift, while the melting enthalpy of all composites is marginally lower than that of the unmodified PBT-PTMO. Similarly, crystallization temperatures (T_c) remain nearly unchanged, and only the system containing the cyanobacterial biomass-based filler (Sp) exhibits a minor shift toward higher T_c and the highest crystallization enthalpy within the series. Nonetheless, all modified composites exhibit lower crystallization enthalpies than the neat matrix, indicating that the presence of modifiers does not reveal nucleation ability on the PBT-PTMO copolymer. Similar trends were previously reported for PTT-PTMO nanocomposites containing low amounts of graphene oxide (GO), in which the T_g of the soft PTMO-rich phase remained unaffected by the nanofiller, indicating preserved chain mobility [9]. Only minor changes in Tm and Tc were observed, and the crystallinity remained comparable to the neat matrix, with slight Tc shifts at higher GO loadings attributed primarily to increased copolymer dispersity rather than filler-induced nucleating effect.

The DSC analysis was complemented by additional experimental attempts to capture changes in the formation of the transcrystalline layer in copolymers and their composites, which are presented in the Supporting Information in Figures S1–S3. The slight variations

in the characteristic phase transition temperatures (T_m, T_c, and T_g) upon incorporation of fillers likely stem from the limited interfacial interactions between the fillers and both polymer matrices. At the current stage of research, given the multitude of factors that affect interfacial interactions and heterogeneous nucleation, it is difficult to clearly identify the dominant factor that distinguishes the crystallization behavior of the two copolymers. Nevertheless, a characteristic feature of the systems in which the formation of a transcrystalline layer was observed was a simultaneous increase in the size of the spherulites in the remaining volume of the polymeric bulk (Supporting information: Figure S1—PBT-PTMO/5% RF and Figure S2—PBF-PTMO/5% Ign). Therefore, degradation- or phase-separation-induced phenomena can be supposed to cause changes in the materials' behavior during melt crystallization. At a loading of 5 wt.%, they may not introduce a sufficient effect to markedly influence chain mobility or crystallization behavior, resulting only in minor thermal shifts. Such subtle effects are consistent with systems in which the modifiers act primarily as inert inclusions rather than active nucleating or segment-restricting agents.

3.5. Thermal Stability

To evaluate the thermal stability and degradation behavior of the considered materials, thermogravimetric analysis (TGA) was performed for both series of composites based on PBF-PTMO and PBT-PTMO block copolymers. To assess how the fillers influence the composites' thermal properties, the onset of degradation (T_{ON}), characteristic temperatures for 5%, 10%, and 50% of weight loss ($T_{5\%}$, $T_{10\%}$, $T_{50\%}$), and temperatures corresponding to the maximum mass-loss rate (T_{DTG}) and residual mass (R) were determined (Table 4). This comparison provides insight into the range of potential thermal limitations and service performance of the composites, as well as the role of bio- and mineral fillers in shaping their decomposition profiles. According to the literature, both copolymers used as matrices exhibit sufficient thermal stability to maintain structural integrity under elevated temperatures, which is essential for applications exposed to thermal fluctuations [5,8]. The PBF-PTMO copolymer obtained via single-step polymerization shows an onset of degradation at approximately 345 °C [8], whereas PBT-PTMO demonstrates slightly higher thermal stability, with degradation temperatures exceeding 350 °C [3]. In the present study, all composites and neat PBT-PTMO exhibited a single decomposition stage (Figure 6), in contrast to the two-stage decomposition observed for PBF-PTMO and other block copolymer systems [5,7,17,84,85].

PBF-PTMO has an onset degradation temperature of 348 °C and $T_{5\%}$ of 354 °C, which is slightly reduced when adding the plant fibers and the Spirulina ($T_{5\%}$ between 341 and 347 °C, with onset temperatures showing no variation, close to 350 °C). On the contrary, the composites with ignimbrite dust show a subtle stabilization effect on the copolymer matrix (PBF-PTMO/5% Ign), with an increase of 12 °C in the onset degradation temperature and of about 6–7 °C in the remaining characteristic temperatures ($T_{5\%}$, $T_{10\%}$, $T_{50\%}$). PBT-PTMO shows higher thermal stability, with an onset degradation temperature of 380 °C, which further decreases for the reed fibers (361 °C). Interestingly, the use of shredded reed reduces the onset temperature to a lesser extent, which might be due to a higher concentration of antioxidant compounds within the biomass (although this is not evidenced in PBF-PTMO composites) or to better compatibility between the polymer and the matrix. Spirulina-filled composites show an onset degradation temperature of 376 °C, close to that of the neat matrix, as well as for ignimbrite-filled samples. The peak temperature of the neat PBF-PTMO copolymer is recorded at 402 °C (24.9%/°C), which is not modified by the mineral dust. The DTG maximum determined for composites containing reed fiber is reduced by only 2–3 °C, while that for shredded reed takes place at 403 °C, compared to the reference copolymer. For both fillers, the maximum degradation rate is slightly lower than that of

the neat matrix (23.8%/°C and 23.3%/°C, respectively). Composites with Spirulina show the peak temperature in the same range, although the maximum rate is lower, 21.8%/°C.

Table 4. TGA data of both series of compositions.

Sample	T_{ON} [°C]	$T_{5\%}$ [°C]	$T_{10\%}$ [°C]	$T_{50\%}$ [°C]	T_{DTG1} [°C]	T_{DTG2} [°C]	R at 700 °C [%]
SERIES I							
PBF-PTMO	348	354	367	399	402	479	1.2
PBF-PTMO/5% Ign	360	360	374	405	400	-	8.1
PBF-PTMO/5% Sp	350	340	363	400	395	-	6.3
PBF-PTMO/5% RF	350	341	360	401	400	-	4.7
PBF-PTMO/5% Reed	349	347	364	402	403	-	2.1
SERIES II							
PBT-PTMO	380	378	389	416	420	-	0.1
PBT-PTMO/5% Ign	378	377	388	414	417	-	4.2
PBT-PTMO/5% Sp	376	368	385	414	416	-	3.2
PBT-PTMO/5% RF	361	354	377	414	416	-	1.0
PBT-PTMO/5% Reed	367	366	383	416	418	-	2.3

T_{ON}—onset temperature; $T_{5\%}$, $T_{10\%}$, and $T_{50\%}$ correspond to the temperatures of 5%, 10%, and 50% mass loss, respectively; T_{DTG1} and T_{DTG2} temperatures corresponding to the maximum of mass losses, R at 700—residue at 700 °C.

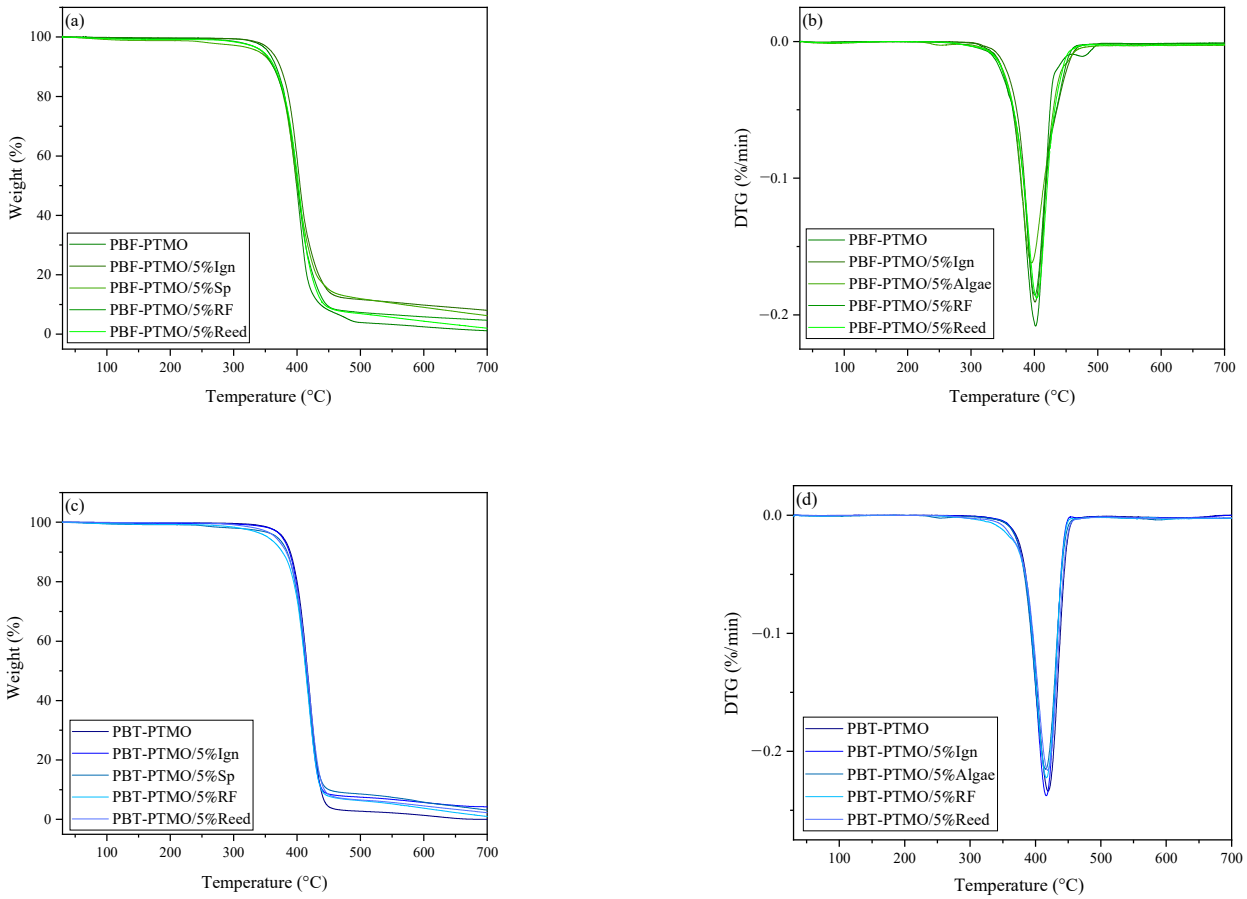

Figure 6. TGA-DTG thermograms for the series of composites based on PBF-PTMO (**a**,**b**), and for the series of composites based on PBT-PTMO (**c**,**d**).

From DTG curves (Figure 6c,d), some differences are also noted in the thermal decomposition of the composites. For instance, PBF-PTMO shows a peak degradation temperature

of 402 °C, with a degradation rate of 21.4%/°C, and a secondary (less intense decomposition effect) at 475 °C (1.8%/°C). For Arundo fillers, there is no modification of the course of the DTG curve, obtaining the same peak temperature and very close degradation rates; the secondary peak, however, shifts to lower temperatures and appears as a shoulder of the main peak. The most distinct behavior is seen for Spirulina composites, with a peak temperature of 393 °C; that is, the main degradation takes place in a narrower range of temperatures. The incorporation of the mineral filler does not seem to affect either the degradation rate or the maximum degradation peak.

Residue at the end of the test shows a slightly higher amount of thermally stable residue for composites than for the neat matrices in both cases, with a particular increase in ignimbrite and Spirulina composites due to the thermal stability of the ignimbrite itself and to the salt content in the Spirulina. Residual mass is close to 8% for PBF-PTMO with ignimbrite and 6% for Spirulina, remaining lower for Arundo-derived materials. A similar trend is found for PBT-PTMO, although at lower values, as also seen for the matrix itself.

Comparable behavior was previously reported for PTF-PTMO (50 wt.%/50 wt.%) nanocomposites obtained via an in situ polymerization method and modified with carbon nanofibers (CNFs) and graphene nanoplatelets (GNPs) [78]. In that system, the onset of thermal degradation, defined as the temperature at 5% mass loss ($T_{5\%}$), increased slightly, by up to 9 °C in an inert atmosphere, upon incorporation of nanoparticles. Under oxidative conditions, however, the differences in T_5% were negligible. The presence of nanoparticles also increased the $T_{10\%}$ and $T_{50\%}$ values, indicating a modest enhancement in thermal stability relative to the unmodified copolyester–ether.

Therefore, the incorporation of the selected modifiers does not adversely affect the processability of the studied copolymers, as the degradation temperatures remain well above those required for typical processing and exploitation operations. At most, the presence of the modifiers may slightly narrow the processing window; however, no detrimental reduction in thermal stability was observed. Overall, the results indicate that the tested modifiers (ignimbrite, cyanobacterial biomass, reed fibers, and reed) are thermally compatible with both copolymer systems, although their ability to enhance thermal resistance is limited at the investigated loading of 5 wt.%.

3.6. Tensile Properties

The incorporation of even small amounts of fillers into a polymer matrix can directly modify its mechanical performance and, in some cases, indirectly influence structural development during processing. The extent of these effects depends not only on the filler content but also on its intrinsic characteristics, such as morphology, chemistry, and interfacial compatibility with the matrix. For this reason, the impact of the selected fillers, ignimbrite, cyanobacterial biomass, and reed residues in the form of fibers and fractionated shredded parts, on the tensile properties and hardness of the PEE-based copolymers was systematically evaluated. All materials exhibited stress–strain curves typical of thermoplastic elastomers, showing facile elongation under low stress, the absence of a clear yield point, and no necking (Figure 7). Such characteristics are consistent with the mechanical response expected for PEE systems with a similar hard-to-soft segment ratio, as previously reported by Kwiatkowska et al. [17], who observed comparable tensile strength and strain at break for both PBF- and PBT-based multiblock copolymers.

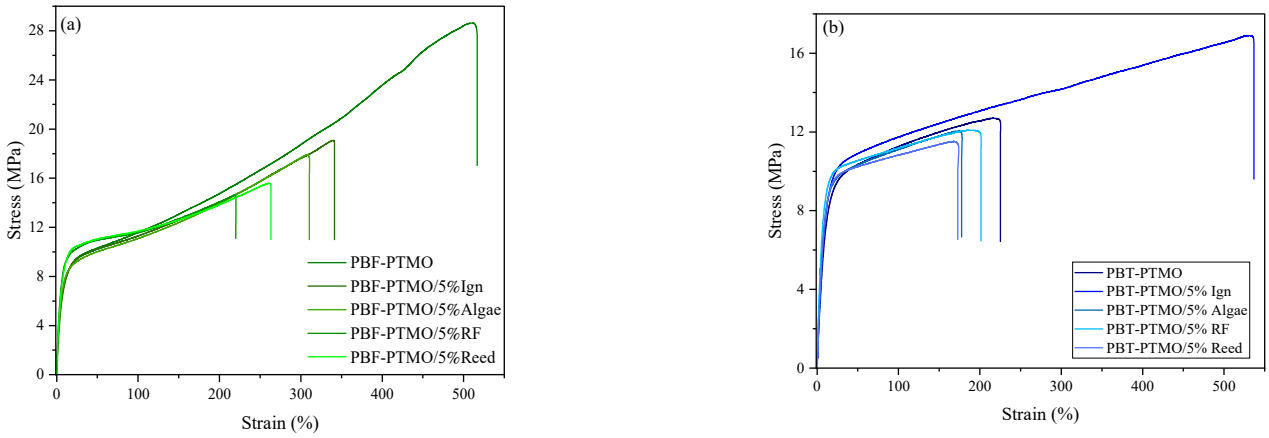

Figure 7. Representative stress–strain curves for for the series of composites based on PBF-PTMO (**a**) and for the series of composites based on PBT-PTMO (**b**).

The series of PBF-PTMO-based composites showed no meaningful change in stress at 100% strain ($\sigma_{100\%}$) upon the addition of any modifier (Table 5, Figure 7a). However, a noticeable reduction in strain at break (from >500% to approximately 250–350%) and a decrease in tensile strength at break were observed, indicating diminished elasticity. This behavior suggests that, despite the presence of rigid fillers, effective stress transfer is not achieved in the PBF-PTMO matrix, and the fillers primarily act as physical constraints that limit macromolecular chain extensibility under large deformation. This effect can be linked to the higher stiffness of the PBF-rich hard phase, which reduces the ability of the segmented structure to reorganize around filler particles, leading to premature failure once the elastic limit of the PTMO-rich soft phase is exceeded [86,87]. Additionally, less favorable dispersion and weaker interfacial adhesion may promote localized stress concentrations, thereby accelerating crack initiation rather than promoting plastic deformation [86].

Table 5. Mechanical properties of the obtained materials.

Sample	$\sigma_{100\%}$ [MPa]	σ_b [MPa]	ε_b [%]	Toughness [MJ/m^3]	H [ShD]
SERIES I					
PBF-PTMO	11.4 ± 0.2	29.2 ± 0.7	536.8 ± 28.4	91.4 ± 4.5	53 ± 1
PBF-PTMO/5% Ign	11.4 ± 0.2	19.0 ± 1.8	337.8 ± 33.0	45.6 ± 0.8	56 ± 1
PBF-PTMO/5% Sp	11.1 ± 0.1	17.9 ± 0.1	379.1 ± 12.3	39.6 ± 1.5	53 ± 1
PBF-PTMO/5% RF	11.5 ± 0.1	15.4 ± 1.0	252.3 ± 37.9	25.9 ± 0.4	54 ± 1
PBF-PTMO/5% Reed	11.4 ± 0.4	16.0 ± 0.5	289.8 ± 23.0	32.5 ± 1.3	54 ± 1
SERIES II					
PBT-PTMO	11.6 ± 0.3	12.8 ± 0.1	227.0 ± 2.6	24.7 ± 0.8	50 ± 1
PBT-PTMO/5% Ign	11.7 ± 0.1	16.0 ± 1.6	474.8 ± 65.5	73.1 ± 1.9	53 ± 1
PBT-PTMO/5% Sp	11.0 ± 0.1	12.4 ± 0.5	227.4 ± 47.3	18.8 ± 0.4	50 ± 1
PBT-PTMO/5% RF	11.0 ± 0.2	11.9 ± 0.3	192.9 ± 20.4	21.9 ± 0.2	51 ± 1
PBT-PTMO/5% Reed	10.9 ± 0.1	11.3 ± 0.3	155.7 ± 18.6	17.8 ± 0.2	51 ± 1

$\sigma_{100\%}$—stress at 100% strain; σ_b and ε_b—stress and strain at break, respectively; toughness calculated by integrating the area under the stress–strain curve; H—hardness according to Shore D.

In contrast, PBT-PTMO-based composites exhibited only minor variations in stress at 100% strain for most incorporated fillers (Figure 7b). Notably, ignimbrite induced a distinct reinforcing effect, simultaneously increasing both tensile strength at break and strain at break, with the latter more than doubling. This unique response indicates a synergistic balance between stiffness and deformability, suggesting efficient stress transfer and delayed

damage accumulation [88]. The enhanced performance can be attributed to a more favorable interaction between ignimbrite particles and the PBT-PTMO matrix, potentially arising from better interphase adhesion, a particle size distribution conducive to homogeneous dispersion, and the high stiffness of ignimbrite, which promotes load redistribution rather than chain immobilization [89]. Moreover, the greater segmental mobility of the PBT hard domains, compared to PBF, likely allows the matrix to accommodate filler-induced stress through plastic deformation rather than brittle fracture. A similar reinforcing and toughening effect has been reported by the authors in elastomeric systems filled with another volcanic-rock-derived filler, basalt powder [90].

In addition, toughness was analyzed as a measure of the material's ability to absorb energy up to fracture and was determined as the area under the stress–strain curve obtained from tensile tests [91,92]. This parameter reflects the resistance to crack initiation and propagation, combining the effects of strength and ductility. For the PBF-PTMO–based series, all composites exhibited lower toughness values, in most cases reduced by more than 50% compared to the neat polymer, consistent with the observed loss of extensibility and limited plastic deformation capability. In contrast, in the PBT-PTMO–based series, only the addition of ignimbrite increased toughness relative to the reference material. The significant (over threefold) increase in toughness for PBT-PTMO containing 5 wt.% of ignimbrite arises from synergistic mechanisms including crack deflection, particle-induced plastic deformation of PBT domains, enhanced hard–soft phase interactions, and additional energy dissipation through controlled interfacial debonding and friction, mechanisms that are absent or ineffective in the neat polymer and in the PBF-PTMO system. Moreover, in addition to the data presented in the Supporting Information, this sample was characterized by significantly smaller spherulitic domains after crystallization under controlled non-isothermal conditions (Figure S2), which may also influence the improvement of the materials' ductility and toughness [93].

In both polymer series, a slight increase in Shore D hardness was observed, particularly in the presence of ignimbrite, which aligns with a modest stiffening effect imparted by the filler. These trends may be contrasted with previous studies on nanofilled multiblock copolymers. For instance, Walkowiak et al. [78] reported that in PTF-PTMO nanocomposites obtained via in situ polymerization, carbon nanofillers significantly increased Young's modulus and tensile strength while decreasing ductility. Similarly, in our earlier work [94], organoclay enhanced modulus and yield stress in PTT-PTMO without loss of elasticity. Moreover, Deng et al. [80] observed that reinforcement in PBF-based composites containing hemp fibers was achieved only at higher filler contents (10–30 wt.%), though at the cost of reduced ductility.

Improvements at low filler loadings are typically observed when using the in situ polymerization method. However, this approach is inherently limited by the maximum amount of filler that can be incorporated—based on our previous work, this value does not exceed approximately 3 wt.% [94]. For this reason, in the present study, the modifiers were introduced via melt blending, which enabled the incorporation of 5 wt.% filler.

Overall, the fillers introduced at this loading caused only limited reinforcement, suggesting that the amount of insoluble material in the polymeric matrix modifier/filler may still be insufficient to generate an effective stress-transfer network within the matrix. This is particularly relevant for complex or irregular bio-derived fillers such as cyanobacterial biomass or reed materials, where interfacial adhesion with the polymer may be inherently weak due to the strong hydrophilic character of the biomass (as observed in SEM analysis), which contradicts the hydrophobic nature of the polymer. Increasing filler content, therefore, appears to be a rational direction for future work, not only to intensify polymer–filler interactions but also to promote filler–filler contacts, which can contribute to the formation

of continuous or quasi-continuous reinforcing pathways. Such structural development could enhance mechanical performance and may additionally support improvements in thermomechanical stability.

3.7. Rheological Behavior

Figure 8 compares the rheological properties of two TPEs differing in the type of rigid domains filled with various plant-based and inorganic fillers. The polymers were tested at different temperatures: 190 °C for PBF-PTMO and 210 °C for PBT-PTMO. Due to the plant component and the risk of lignocellulose degradation, which could interfere with the measurement, the materials were tested at the lowest possible temperature. The measurement temperatures were selected considering the processing temperatures used, increased by 5 °C. For PBT-PTMO, preliminary measurements were attempted at 190 °C and 200 °C, but in both cases, elastic properties dominated over viscous behavior over the entire tested range. In the selected temperature set, it was possible to compare the behavior of the materials in the molten state. Additionally, the results of measurements performed at 190 °C for PBT-PTMO are summarized in the Supporting Information.

The complex viscosity curves (Figure 8a,b) of both composite series, varying with rigid copolymer phase content, show similar trends when particle-shaped fillers (IG, Reed) are used. The introduction of Ign as a fine, inorganic, particle-shaped filler did not significantly affect the rheological behavior of the composites. All the rheological curves, as well as the complex viscosity values over the entire ω range for both TPE matrices, are comparable to those of the unmodified copolymers. Similar results, showing a slight reduction in polymer viscosity after the introduction of a small amount of a different basalt powder (5 wt.%) into polypropylene [95], were obtained in our previous studies. The opposite effect, a reduction in complex viscosity, was observed for the Sp-filled series. The viscosity-lowering impact of these materials can be assumed to be related to the low thermal stability of the filler [48] and the possible effect of low-molecular-weight decomposition products. The shape of the $\eta^*(\omega)$ and $G'(\omega)$ curves (Figure 8c,d) suggests exceeding the rheological threshold of filler percolation in the polymer matrix. The occurrence of three-dimensional structures of fillers in mutual contact was observed in the case of PBF-based composites for RF- and Sp-filled series. The changes in the curve's shape are related to the observed increase in complex viscosity and the disappearance or reduction in the G′ of ω dependence at the terminal range at low ω values. In the case of natural fibers with a high aspect ratio and reed with a significantly higher share of large-dimensional particles compared to Ign and Sp, this effect is visible in semi-transparent samples. In the case of the Sp-filled series, it may be caused by agglomeration of the thermally stable Spirulina fraction [96], which reorganizes in the polymer matrix during long-term thermal exposure. In all cases except PBF-PTMO filled with RF, the G″ value exceeded G′, confirming the dominant viscous behavior and the properly selected processing conditions.

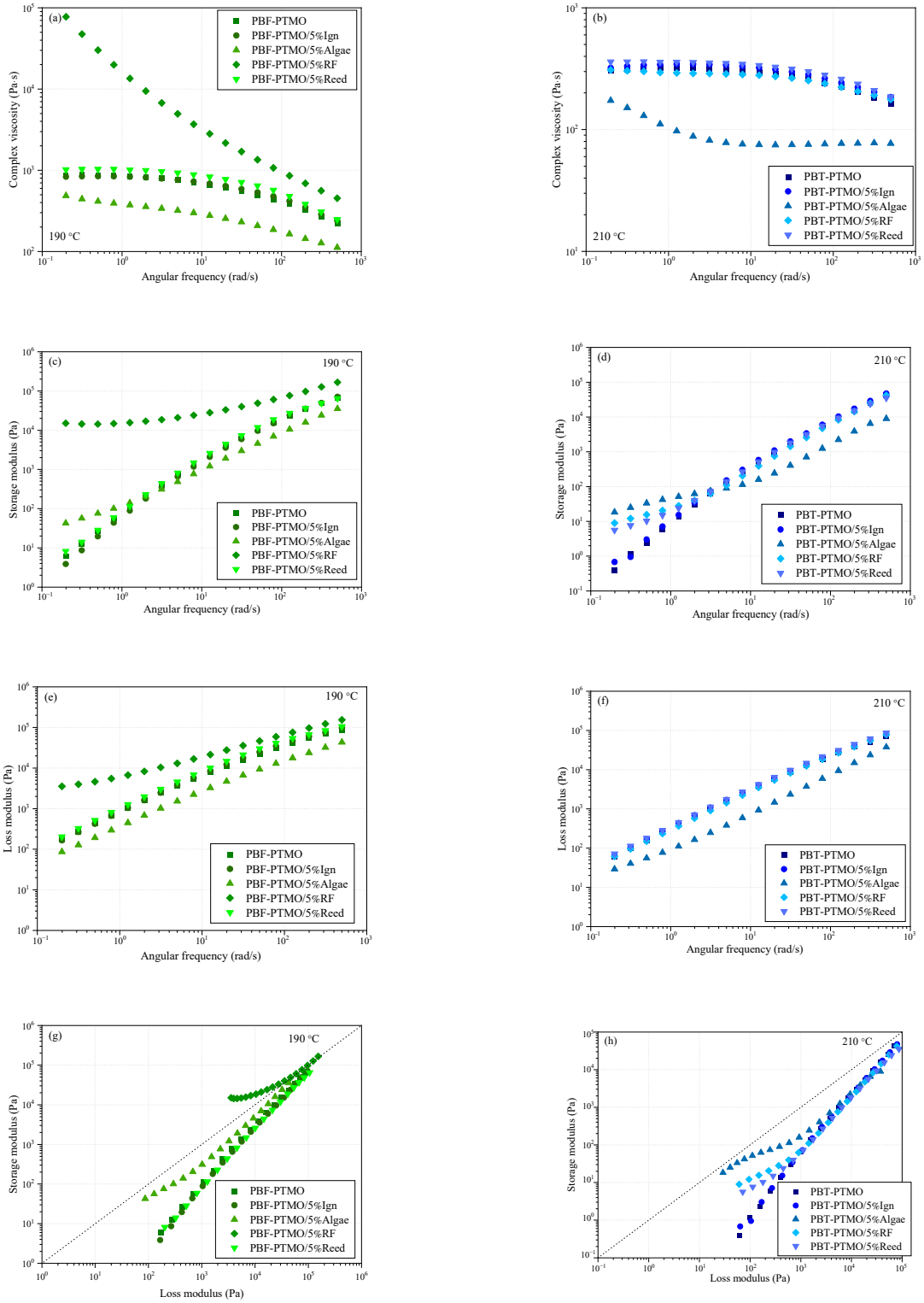

Figure 8. Results of rheological analysis of PBF/PBT-PTMO and their composites: complex viscosity curves (**a**,**b**); storage (**c**,**d**) and loss (**e**,**f**) modulus vs. angular frequency; Han–Chuang plots (**g**,**h**).

The Han–Chuang plot (HC) representing the G′ vs. G″ comparison is an interpretation of data from oscillatory rheological analysis, which may be related both to changes in the rheological behavior of the melt induced by microstructure development and the compatibility of the components when tested at constant temperature [97,98]. Except for PBF-PTMO filled with reed fibers, the curves for the remaining materials are located below the G′=G″ line, which indicates the dominant quasi-liquid state of those materials

during measurement [99]. Both polymers, modified with an inorganic filler (Ign) and the PBF-PTMO series containing shredded reed, showed comparable slopes in the HC plot. The introduction of Sp resulted in a reduced slope at lower values of angular frequencies for PBF-based composites. The change in the HC-plot slope is related to the material's more heterogeneous structure compared to the unfilled copolymer. According to Zhou et al. [100], the observed inflection point of the curve for PBT-PTMO may be related to a higher degree of composition heterogeneity and a stronger physical polymer–filler interfacial interaction. Considering the higher measurement and processing temperature of the PBT-based copolymer composition, it can be assumed that this is related to a greater degree of thermal decomposition of the cyanobacterial biomass filler and the proportion of the dispersed, thermally transformed, temperature-stable phase and salt residue in the polymer. The solid-like behavior of the HC-plot of PBF-PTMO with 5 wt.% RF is attributed to exceeding the rheological percolation threshold and to strong physical interactions that interlock natural fibers within the molten polymeric matrix [100]. The occurrence of these phenomena suggests a significant increase in complex viscosity and a flattening of the storage modulus curve at low angular frequencies [101,102].

To summarize, the effect of fillers introduced at the same concentration into two TPE matrices on changes in rheological behavior, as assessed by oscillatory rheometry, can be attributed to two groups of phenomena. The first one is related to the geometric characteristics of the fillers, namely particle size and aspect ratio (Ign < Sp < Reed < RF). In the case of a well-dispersed inorganic filler (Ign) composite, no agglomeration of the filler occurred, and the rheological characteristics for composites made with both polymers did not change significantly. Moreover, the presence of Reed particles, with a size an order of magnitude larger than Ign, caused the composite materials to differ only slightly in characteristics from the reference samples (PBT-PTMO/5% Reed). Only in the case of the fibrous filler (RF) for both TPE matrices, a prominent change in the rheological curves was observed (more pronounced for the PBF-PTMO series), indicating the formation of interactions between the high-aspect-ratio filler particles in the molten polymeric bulk. However, differences in the intensity of rheological behavior changes may result from different test temperatures, reflecting the melt processing conditions. The second factor influencing changes in the rheological properties of the analyzed materials was degradation, which led to a significant decrease in the viscosity of compositions containing SP, as exemplified by the thermosensitive filler with low thermal stability.

4. Conclusions

This work provides a comprehensive evaluation of how bio-derived and mineral fillers influence the performance of two chemically distinct thermoplastic elastomer systems. Overall, the comparative analysis shows that the type, morphology, and origin of natural fillers strongly affect the extent to which the structural, thermal, rheological, and mechanical properties of TPEs are modified, with biobased and petroleum-derived matrices responding differently to the same modifiers. These findings highlight both the potential and the limitations of incorporating low loadings of diverse natural fillers into multiblock copolymers and offer guidance for designing more sustainable TPE composites with tailored performance. NMR analysis confirms the successful incorporation of PTMO into both PBF-PTMO and PBT-PTMO copolymer matrices, with all characteristic signals matching the expected chemical structures. The minor discrepancies between theoretical and calculated flexible-segment contents (3.7% for PBF-PTMO and 1.5% for PBT-PTMO) indicate only minor deviations in composition, likely arising from processing-related PTMO losses. Scanning electron microscopy (SEM) revealed a two-phase structure for both copolymers, as is usual for TPEs, with good compatibility between the rigid and flexible segments. A

different behavior was observed for the various fillers in both matrices; for instance, in PBF-PTMO composites, the ignimbrite dust is found mainly as clusters; in PBT-PTMO, the dust is uniformly dispersed; and in *Spirulina*-containing composites, a uniform distribution is found for both matrices, together with the formation of well-defined crystalline structures in the form of dendrites. Reed composites show a similar morphology for both copolymers, with the appearance of dendritic structures, indicating that both biobased fillers could promote the crystallization of both matrices. FTIR spectroscopy further verifies the expected chemical structures of both matrices, showing all characteristic bands of the polyester–PTMO systems. The absence of new absorption features upon filler addition indicates no detectable chemical interactions at a loading of 5 wt.%, while still suggesting good dispersion of the fillers within the polymer matrices. DSC analysis demonstrates that introducing 5 wt.% modifiers into both TPE systems results in only minor alterations to their thermal behavior, with the main transition temperatures (T_g, T_c, T_m) remaining largely unchanged. Subtle increases in crystallization or melting enthalpy observed for selected PBF-PTMO composites suggest a weak nucleating or crystallization-promoting effect, in good agreement with SEM findings, whereas the PBT-PTMO series shows an even more limited response. Overall, these modest thermal shifts indicate that, at this loading, the modifiers behave primarily as inert inclusions, without significantly disrupting chain mobility or crystallization processes. Mechanical testing reveals that the incorporation of 5 wt.% fillers provides only limited reinforcement in both copolymer matrices, with most composites retaining the characteristic elastomeric behavior of PEE systems. While ignimbrite induces a measurable strengthening effect, particularly in the PBT-PTMO series, due to the better particle distribution within the matrix, the remaining modifiers either reduce ductility or exert only a marginal influence, indicating insufficient stress-transfer efficiency at the studied loading. These results suggest that higher filler contents or improved polymer–filler interfacial compatibility will be required to establish a more effective reinforcing network and achieve meaningful improvements in mechanical performance. Moreover, rheological analysis shows that adding 5 wt.% fillers generally leads to minor changes in the melt flow behavior of both TPE systems when particle-shaped inorganic or plant-derived fillers are used, with ignimbrite in particular leaving complex viscosity essentially unaffected. In contrast, fillers with higher aspect ratios or more heterogeneous particle size distributions, such as reed fibers or Spirulina, exhibit rheological percolation, evidenced by increased complex viscosity, modified terminal behavior, and altered HC-plot slopes, reflecting the formation of three-dimensional filler–filler physical networks in the melt. Overall, these results indicate that while most fillers behave as inert inclusions under the tested conditions, selected bio-derived modifiers can induce limited structural connectivity in the molten state, subtly shifting the viscoelastic response toward more heterogeneous or partially solid-like behavior.

From an application perspective, the results indicate that specific filler–matrix combinations can be tailored to distinct use scenarios. Composites based on PBT-PTMO containing ignimbrite dust, combining good filler dispersion, enhanced tensile strength, and preserved elastomeric behavior with minimal impact on processability, are suitable for applications such as flexible seals, gaskets, and elastomeric technical components requiring high elasticity and mechanical robustness. Composites containing Spirulina or reed-derived fillers, which promote crystallization and induce melt-state structuring, are better suited for extrusion- or foaming-based applications that require improved shape stability and controlled flow. In contrast, PBF-PTMO composites with bio-derived fillers are promising for low-load-bearing applications where sustainability and increased bio-based content are prioritized, such as packaging or consumer products.

Future work should focus either on increasing filler loadings or optimizing surface modification strategies to enhance polymer–filler interactions and promote the formation of more effective reinforcing networks. In addition, exploring alternative bio-based fillers, compatibilizers, and processing routes may further improve the balance of mechanical, thermal, and rheological properties, enabling the development of next-generation sustainable TPE composites.

Supplementary Materials: The following Supporting Information can be downloaded at https://www.mdpi.com/article/10.3390/polym18040513/s1, S.I. 1. Supplementing characterization methods; S.I. 2. Supplementing results and comments: S.I. 2.1. Polarized light microscopy of samples crystallized in controlled conditions; Figure S1: Polarized light microscopy images of PBT- and PBF-PTMO and their composites obtained by cooling at the heating stage in controlled cooling rate of 5 °C/min; Figure S2: Polarized light microscopy images of PBF-PTMO/5%Ign and PBF-PTMO/5%Ign composites obtained by cooling at the heating stage in controlled cooling rates of 10, 5, and 2 °C/min, taken with a magnification of ×100; Figure S3: Polarized light microscopy images of PBT- and PBF-PTMO/5%Ign composites obtained by cooling at the heating stage in controlled cooling rate of 2 °C/min, taken with a magnification of ×200.

Author Contributions: Conceptualization, S.P. and Z.O.; investigation, S.P., Z.O., K.W., I.I., A.P. and M.B.; writing—original draft preparation, S.P., Z.O. and M.B.; writing—review and editing, S.P., Z.O. and M.B. All authors have read and agreed to the published version of the manuscript.

Funding: This research was funded by the Ministry of Science, Innovation and Universities of Spain within the Rock'n'Rot Project (PID2023-149534NA-I00, MCIU/AEI/10.13039/501100011033/FEDER, UE).

Data Availability Statement: The data presented in this study are available on request from the corresponding author.

Conflicts of Interest: The authors declare no conflicts of interest.

References

1. Drobny, J.G. *Handbook of Thermoplastic Elastomers*; Plastic Design Library, William Andrews Inc.: Norwich, CT, USA, 2007.
2. Legge, N.L. Thermoplastic Elastomers Today. In *Thermoplastic Elastomers II: Processing for Performance*; Rapra Technology Limited: Shropshire, UK, 1989.
3. Hao, T.; Zhang, C.; Hu, G.; Jiang, T.; Zhang, Q. Effects of Co-hard Segments on the Microstructure and Properties Thermoplastic Poly(ether ester) Elastomers. *J. Appl. Polym. Sci.* **2016**, *133*, 43337. [CrossRef]
4. Szymczyk, A.; Nastalczyk, J.; Sablong, R.J.; Roslaniec, Z. The Influence of Soft Segment Length on Structure and Properties of Poly(trimethylene terephthalate)-block-Poly(tetramethylene oxide) Segmented Random Copolymers. *Polym. Adv. Technol.* **2011**, *22*, 72–83. [CrossRef]
5. Xu, Q.; Chen, J.; Huang, W.; Qu, T.; Li, X.; Li, Y.; Yang, X.; Tu, Y. One Pot, One Feeding Step, Two-Stage Polymerization Synthesis and Characterization of (PTT-b-PTMO-b-PTT)n Multiblock Copolymers. *Macromolecules* **2013**, *46*, 7274–7281. [CrossRef]
6. Celebi, H.; Bayram, G.; Dogan, A. Effect of ZnO Type and Concentration on the Mophology, Thermal, and Mechanical Properties of Poly(ether ester)/ZnO Composites. *J. Appl. Polym. Sci.* **2013**, *129*, 3417–3424. [CrossRef]
7. Celebi, H.; Bayram, G.; Dogan, A. Influence of Zinc Oxide on Thermoplastic Elastomer-based Composites: Synthesis, Processing, Structural, and Thermal Characterization. *Polym. Compos.* **2016**, *37*, 2369–2376. [CrossRef]
8. Huang, W.; Wan, Y.; Chen, J.; Xu, Q.; Li, X.; Yang, X.; Li, Y.; Tu, Y. One Pot Synthesis and Characterization of Novel Poly(ether ester) Mutiblock Copolymers Containing Poly(tetramethylene oxide) and Poly(ethylene terephthalate). *Polym. Chem.* **2014**, *5*, 945–954. [CrossRef]
9. Paszkiewicz, S.; Szymczyk, A.; Špitalský, Z.; Mosnáček, J.; Kwiatkowski, K.; Rosłaniec, Z. Structure and Properties of Nanocomposites Based on PTT-Block-PTMO Copolymer and Graphene Oxide Prepared by in Situ Polymerization. *Eur. Polym. J.* **2014**, *50*, 69–77. [CrossRef]
10. Long, T.E. *Modern Polyesters: Chemistry and Technology of Polyesters and Copolyesters*; John Wiley and Sons: Hoboken, NJ, USA, 2004.

11. Poulopoulou, N.; Kantoutsis, G.; Bikiaris, D.N.; Achilias, D.S.; Kapnisti, M.; Papageorgiou, G.Z. Biobased Engineering Thermoplastics: Poly(butylene 2,5-furandicarboxylate) Blends. *Polymers* **2019**, *11*, 937. [CrossRef]
12. Huang, W.; Pan, Q.; Qi, H.; Li, X.; Tu, Y.; Li, C.Y. Poly(butylene terephthalate)-b-Poly(ethylene oxide) Alternating Multiblock Copolymers: Synthesis and Application in Solid Polymer Electrolytes. *Polymer* **2017**, *128*, 188–199. [CrossRef]
13. Chen, J.; Chen, D.; Huang, W.; Yang, X.; Li, X.; Tu, Y.; Zhu, X. A One Pot Facile Synthesis of Poly(butylene terephthalate)-block-Poly(tetramethylene oxide) Alternative Multiblock Copolymers via PROP Method. *Polymer* **2016**, *107*, 29–36. [CrossRef]
14. Schmalz, H.; van Guldener, V.; Gabriëlse, W.; Lange, R.; Abetz, V. Morphology, Surface Structure, and Elastic Properties of PBT-Based Copolyesters with PEO-b-PEB-b-PEO Triblock Copolymer Soft Segments. *Macromolecules* **2002**, *35*, 5491–5499. [CrossRef]
15. Papageorgiou, G.Z.; Tsanaktsis, V.; Papageorgiou, D.G.; Exarhopoulos, S.; Papageorgiou, M.; Bikiaris, D.N. Evaluation of Polyesters from Renewable Resources as Alternatives to the Current Fossil-Based Polymers. Phase Transitions of Poly(butylene 2,5-furan-dicarboxylate). *Polymer* **2014**, *55*, 3846–3858. [CrossRef]
16. Zhu, J.; Cai, J.; Xie, W.; Chen, P.-H.; Gazzano, M.; Scandola, M.; Gross, R.A. Poly(butylene 2,5-furan dicarboxylate), a Biobased Alternative to PBT: Synthesis, Physical Properties, and Crystal Structure. *Macromolecules* **2013**, *46*, 796–804. [CrossRef]
17. Kwiatkowska, M.; Kowalczyk, I.; Rozwadowski, Z.; Piesowicz, E.; Szymczyk, A. Hytrel-like Copolymers Based on Furan Polyester: The Effect of Poly(butylene furanoate) Segment on Microstructure and Mechanical/Elastic Performance. *Molecules* **2023**, *28*, 2962. [CrossRef]
18. Papageorgiou, G.Z.; Papageorgiou, D.G.; Terzopoulou, Z.; Bikiaris, D.N. Production of Bio-Based 2,5-Furan Dicarboxylate Polyesters: Recent Progress and Critical Aspects in Their Synthesis and Thermal Properties. *Eur. Polym. J.* **2016**, *83*, 202–229. [CrossRef]
19. Koo, J.M.; Kang, J.; Shin, S.H.; Jegal, J.; Cha, H.G.; Choy, S.; Hakkarainen, M.; Park, J.; Oh, D.X.; Hwang, S.Y. Biobased Thermoplastic Elastomer with Seamless 3D-Printability and Superior Mechanical Properties Empowered by in-Situ Polymerization in the Presence of Nanocellulose. *Compos. Sci. Technol.* **2020**, *185*, 107885. [CrossRef]
20. Miah, M.R.; Mahmud, S.; Khan, A.N.; Jalil, M.A.; Wang, J.; Zhu, J. Recent Advances in Sustainable Thermoplastic Polyester Elastomers: Synthesis, Properties and Applications. *Polymer* **2025**, *336*, 128878. [CrossRef]
21. Zhang, Y.; Han, X.; Wang, R.; Qu, C.; Ren, C.; Chen, H.; Yin, P. Bio-Based Functional Monomer-Based High Thermal and Mechanical Performance TPEE. *Eur. Polym. J.* **2025**, *236*, 114105. [CrossRef]
22. Fei, X.; Wang, J.; Zhang, X.; Jia, Z.; Jiang, Y.; Liu, X. Recent Progress on Bio-Based Polyesters Derived from 2,5-Furandicarbonxylic Acid (FDCA). *Polymers* **2022**, *14*, 625. [CrossRef]
23. Lalanne, L.; Nyanhongo, G.S.; Guebitz, G.M.; Pellis, A. Biotechnological Production and High Potential of Furan-Based Renewable Monomers and Polymers. *Biotechnol. Adv.* **2021**, *48*, 107707. [CrossRef]
24. Loos, K.; Zhang, R.; Pereira, I.; Agostinho, B.; Hu, H.; Maniar, D.; Sbirrazzuoli, N.; Silvestre, A.J.D.; Guigo, N.; Sousa, A.F. A Perspective on PEF Synthesis, Properties, and End-Life. *Front. Chem.* **2020**, *8*, 585. [CrossRef] [PubMed]
25. Sousa, A.F.; Patrício, R.; Terzopoulou, Z.; Bikiaris, D.N.; Stern, T.; Wenger, J.; Loos, K.; Lotti, N.; Siracusa, V.; Szymczyk, A.; et al. Recommendations for Replacing PET on Packaging, Fiber, and Film Materials with Biobased Counterparts. *Green Chem.* **2021**, *23*, 8795–8820. [CrossRef]
26. Agostinho, B.; Silvestre, A.; Sousa, A.F. From PEF to RPEF: Disclosing the Potential of Deep Eutectic Solvents in Biobased Polyesters Continuous de-/Re-Polymerization Recycling. *Green Chem.* **2022**, *24*, 3115–3119. [CrossRef]
27. Li, X.-L.; Fu, T.; Li, Z.-M.; Li, Y.; Wang, X.-L.; Wang, Y.-Z. A Synchronously Chemically Closed-Loop and High-Performance Approach for Furan-Based Copolyesters with Robustness, High Gas Barriers, and High Puncture Resistance. *Green Chem.* **2022**, *24*, 8552–8561. [CrossRef]
28. Agostinho, B.; Irska, I.; Kwiatkowska, M.; Szymczyk, A.; Silvestre, A.J.D.; Sousa, A.F. Optimized Closed-Loop Recycling of Bio-Based Poly(trimethylene 2,5-furandicarboxylate) Using Eutectic Solvents. *Sustain. Mater. Technol.* **2025**, *45*, e01506. [CrossRef]
29. Guidotti, G.; Soccio, M.; Siracusa, V.; Gazzano, M.; Munari, A.; Lotti, N. Novel Random Copolymers of Poly(butylene 1,4-cyclohexane dicarboxylate) with Outstanding Barrier Properties for Green and Sustainable Packaging: Content and Length of Aliphatic Side Chains as Efficient Tools to Tailor the Material's Final Performance. *Polymers* **2018**, *10*, 866. [CrossRef]
30. Guidotti, G.; Soccio, M.; Lotti, N.; Gazzano, M.; Siracusa, V.; Munari, A. Poly(propylene 2,5-thiophenedicarboxylate) vs. Poly(propylene 2,5-furandicarboxylate): Two Examples of High Gas Barrier Bio-Based Polyesters. *Polymers* **2018**, *10*, 785. [CrossRef]
31. Guidotti, G.; Soccio, M.; García-Gutiérrez, M.C.; Ezquerra, T.; Siracusa, V.; Gutiérrez-Fernández, E.; Munari, A.; Lotti, N. Fully Biobased Superpolymers of 2,5-Furandicarboxylic Acid with Different Functional Properties: From Rigid to Flexible, High Performant Packaging Materials. *ACS Sustain. Chem. Eng.* **2020**, *8*, 9558–9568. [CrossRef]

32. Jacquel, N.; Saint-Loup, R.; Pascault, J.P.; Rousseau, A.; Fenouillot, F. Bio-Based Alternatives in the Synthesis of Aliphatic–Aromatic Polyesters Dedicated to Biodegradable Film Applications. *Polymer* **2015**, *59*, 234–242. [CrossRef]
33. Zhou, W.; Zhang, Y.; Xu, Y.; Wang, P.; Gao, L.; Zhang, W.; Ji, J. Synthesis and Characterization of Bio-Based Poly(butylene furandicarboxylate)-b-Poly(tetramethylene glycol) Copolymers. *Polym. Degrad. Stab.* **2014**, *109*, 21–26. [CrossRef]
34. Wu, B.; Xu, Y.; Bu, Z.; Wu, L.; Li, B.G.; Dubois, P. Biobased Poly(butylene 2,5-furandicarboxylate) and Poly(butylene adipate-co-butylene 2,5-furandicarboxylate)s: From Synthesis Using Highly Purified 2,5-Furandicarboxylic Acid to Thermo-Mechanical Properties. *Polymer* **2014**, *55*, 3648–3655. [CrossRef]
35. Ercan, N.; Durmus, A. Structure–Property Relationships and Constitutive Viscoelastic Behaviors of Polyether-Block-amide Elastomers in Melt and Solid States. *J. Appl. Polym. Sci.* **2022**, *139*, e52458. [CrossRef]
36. Yilgor, E.; Isik, M.; Yilgor, I. Novel Synthetic Approach for the Preparation of Poly(urethaneurea) Elastomers. *Macromolecules* **2010**, *43*, 8588–8593. [CrossRef]
37. Wilson, R.; Divakaran, A.V.; S, K.; Varyambath, A.; Kumaran, A.; Sivaram, S.; Ragupathy, L. Poly(glycerol sebacate)-Based Polyester–Polyether Copolymers and Their Semi-Interpenetrated Networks with Thermoplastic Poly(ester–ether) Elastomers: Preparation and Properties. *ACS Omega* **2018**, *3*, 18714–18723. [CrossRef]
38. Su, Y.; Yu, J.; Wang, Y.; Zhu, J.; Hu, Z. Effect of Hard Segment Length on the Properties of Poly(ether ester) Elastomer Prepared by One Pot Copolymerization of Poly(ethylene glycol) and Cyclic Butylene Terephthalate. *J. Polym. Res.* **2015**, *22*, 193. [CrossRef]
39. Kim, S.B.; Kim, H.R.; Nam, B.U. Miscibility, Thermal, Morphological and Mechanical Behaviour of Polycarbonate/Poly(trimethylene terephthalate)Blends with Poly(butylene adipate-co-terephthalate) as a Compatibilizer. *Asian J. Chem.* **2013**, *25*, 5143–5146. [CrossRef]
40. Paszkiewicz, S.; Szymczyk, A.; Livanov, K.; Wagner, H.D.; Rosłaniec, Z. Enhanced Thermal and Mechanical Properties of Poly(trimethylene terephthalate-block-Poly(tetramethylene oxide) Segmented Copolymer Based Hybrid Nanocomposites Prepared by in Situ Polymerization via Synergy Effect between SWCNTs and Graphene Nanoplatelets. *Express Polym. Lett.* **2015**, *9*, 509–524. [CrossRef]
41. Paszkiewicz, S.; Szymczyk, A.; Pilawka, R.; Przybyszewski, B.; Czulak, A.; RosŁaniec, Z. Improved Thermal Conductivity of Poly(trimethylene terephthalate-block-Poly(tetramethylene oxide) Based Nanocomposites Containing Hybrid Single-Walled Carbon Nanotubes/Graphene Nanoplatelets Fillers. *Adv. Polym. Technol.* **2017**, *36*, 236–242. [CrossRef]
42. Xie, H.; Lu, H.; Zhang, Z.; Li, X.; Yang, X.; Tu, Y. Effect of Block Number and Weight Fraction on the Structure and Properties of Poly(butylene terephthalate)-block-Poly(tetramethylene oxide) Multiblock Copolymers. *Macromolecules* **2021**, *54*, 2703–2710. [CrossRef]
43. Jagadeesh, P.; Puttegowda, M.; Boonyasopon, P.; Rangappa, S.M.; Khan, A.; Siengchin, S. Recent Developments and Challenges in Natural Fiber Composites: A Review. *Polym. Compos.* **2022**, *43*, 2545–2561. [CrossRef]
44. Mori, R. Replacing All Petroleum-Based Chemical Products with Natural Biomass-Based Chemical Products: A Tutorial Review. *RSC Sustain.* **2023**, *1*, 179–212. [CrossRef]
45. Romero, F.; Luis, S.; Díaz, S.; Ortega, Z. Rotomolded Polypropylene-Ignimbrite Composites: Giving a Second Life to Mineral Dust Wastes. *Polym. Compos.* **2024**, *46*, 6594–6608. [CrossRef]
46. Díaz, S.; Romero, F.; Suárez, L.; Tcharkhtchi, A.; Ortega, Z. A Preliminary Study on the Use of Microalgae Biomass as a Polyolefin Stabilizer. *Iran. Polym. J.* **2025**, *34*, 2183–2193. [CrossRef]
47. Suárez, L.; Barczewski, M.; Kosmela, P.; Marrero, M.D.; Ortega, Z. Giant Reed (*Arundo donax* L.) Fiber Extraction and Characterization for Its Use in Polymer Composites. *J. Nat. Fibers* **2023**, *20*, 2131687. [CrossRef]
48. Díaz, S.; Romero, F.; Suárez, L.; Ortega, Z. A Preliminary Assessment on the Preparation of Spirulina/PE Blends by Compression Molding. *Compos. Theory Pract.* **2024**, *24*, 238–245. [CrossRef]
49. Suárez, L.; Billham, M.; Garrett, G.; Cunningham, E.; Marrero, M.D.; Ortega, Z. A New Image Analysis Assisted Semi-Automatic Geometrical Measurement of Fibers in Thermoplastic Composites: A Case Study on Giant Reed Fibers. *J. Compos. Sci.* **2023**, *7*, 326. [CrossRef]
50. *PN-EN 60811-501*; Cables and Optical Fibre Cables—Test Methods for Non-Metallic Materials—Part 501: Mechanical Tests—Verification of the Mechanical Properties of Insulating and Sheathing Compounds. Polish Committee for Standardization: Warsaw, Poland, 2012.
51. *ISO 527*; Plastics—Determination of Tensile Properties—Part 1: General Principles. ISO: Geneva, Switzerland, 2019.
52. Han, J.-H.; Zhang, H.; Chen, M.-J.; Wang, G.-R.; Zhang, Z. CNT Buckypaper/Thermoplastic Polyurethane Composites with Enhanced Stiffness, Strength and Toughness. *Compos. Sci. Technol.* **2014**, *103*, 63–71. [CrossRef]
53. Jiang, Y.; Woortman, A.J.J.; Alberda Van Ekenstein, G.O.R.; Loos, K. A Biocatalytic Approach towards Sustainable Furanic-Aliphatic Polyesters. *Polym. Chem.* **2015**, *6*, 5198–5211. [CrossRef]

54. Papadopoulos, L.; Xanthopoulou, E.; Nikolaidis, G.N.; Zamboulis, A.; Achilias, D.S.; Papageorgiou, G.Z.; Bikiaris, D.N. Towards High Molecular Weight Furan-Based Polyesters: Solid State Polymerization Study of Bio-Based Poly(propylene furanoate) and Poly(butylene furanoate). *Materials* **2020**, *13*, 4880. [CrossRef]
55. Zhou, J.; Jiang, Z.; Wang, Z.; Zhang, J.; Li, J.; Li, Y.; Zhang, J.; Chen, P.; Gu, Q. Synthesis and Characterization of Triblock Copolymer PLA-b-PBT-b-PLA and Its Effect on the Crystallization of PLA. *RSC Adv.* **2013**, *3*, 18464. [CrossRef]
56. Zhang, X.; Ma, S.; Shen, A.; Zhu, J.; Shen, Z.; Wang, J.; Liu, X. High Molecular Weight Poly(butylene terephthalate-co-butylene 2,5-furan dicarboxylate) Copolyesters: From Synthesis to Thermomechanical and Barrier Properties. *J. Appl. Polym. Sci.* **2020**, *137*, 49365. [CrossRef]
57. Walkowiak, K.; Irska, I.; Zubkiewicz, A.; Rozwadowski, Z.; Paszkiewicz, S. Influence of Rigid Segment Type on Copoly(ether-ester) Properties. *Materials* **2021**, *14*, 4614. [CrossRef]
58. Paszkiewicz, S.; Irska, I.; Zubkiewicz, A.; Szymczyk, A.; Piesowicz, E.; Rozwadowski, Z.; Goracy, K. Biobased Thermoplastic Elastomers: Structure-Property Relationship of Poly(hexamethylene 2,5-furanodicarboxylate)-block-Poly(tetrahydrofuran) Copolymers Prepared by Melt Polycondensation. *Polymers* **2021**, *13*, 397. [CrossRef] [PubMed]
59. Cao, Y.; Zhu, P.; Zhou, Y.; Wang, D.; Dong, X. Influence of Soft Block and Film Thickness on Confined Morphology of Poly(ether-mb-amide) Multiblock Copolymers. *Polym. Cryst.* **2020**, *3*, e10100. [CrossRef]
60. Tudryn, G.J.; O'Reilly, M.V.; Dou, S.; King, D.R.; Winey, K.I.; Runt, J.; Colby, R.H. Molecular Mobility and Cation Conduction in Polyether–Ester–Sulfonate Copolymer Ionomers. *Macromolecules* **2012**, *45*, 3962–3973. [CrossRef]
61. Szymczyk, A. Poly(trimethylene terephthalate-block-tetramethylene oxide) Elastomer/Single-walled Carbon Nanotubes Nanocomposites: Synthesis, Structure, and Properties. *J. Appl. Polym. Sci.* **2012**, *126*, 796–807. [CrossRef]
62. Yates, J.T.; Madey, T.E. *Vibrational Spectroscopy of Molecules on Surfaces*; Spinger: Moscow, Russia, 1987; Volume 1.
63. Mao, H.-I.; Chen, C.-W.; Rwei, S.-P. Synthesis and Nonisothermal Crystallization Kinetics of Poly(butylene terephthalate-co-tetramethylene ether glycol) Copolyesters. *Polymers* **2020**, *12*, 1897. [CrossRef]
64. Najjar, K.; Bridge, C.M. Characterization of Glitter Cosmetic Particles Using FT-IR Spectroscopy. *Spectroscopy* **2018**, *33*, 30–37.
65. Wang, G.; Dong, Y.; Hao, X.; Zhang, L.; Sun, R. Bio-Based Poly(butylene furandicarboxylate-co-butylene 2,5-thiophenedicarboxylate): Synthesis, Thermal Properties, Crystallization Properties and Mechanical Properties. *Polym. Bull.* **2023**, *80*, 5373–5395. [CrossRef]
66. Fakirov, S. *Handbook of Thermoplastic Polyesters: Homopolymers, Copolymers, Blends, and Composites*; Wiley-VCH Verlag GmbH & Co. KGaA: Weinheim, Germany, 2002; pp. 1–57.
67. Fakirov, S. *Handbook of Condensation Thermoplastic Elastomers*; Wiley-VCH Verlag GmbH & Co. KGaA: Weinheim, Germany, 2006; pp. 1–619. [CrossRef]
68. Liu, F.; Yao, M.; Run, M. Synthesis and Characterizations of Poly(trimethylene terephthalate)-b-Poly(tetramethylene glycol) Copolymers. *Int. J. Polym. Sci.* **2013**, *2013*, 156289. [CrossRef]
69. Zhu, J.; Liang, Y.; Si, W.; Zhang, S. Bubblegum Inspired Epoxidized Natural Rubber Composites for Superior Mechanical and Electrical Properties. *Polymer* **2022**, *257*, 125286. [CrossRef]
70. Nie, W.-C.; Xiao, Q.; Wu, J.-M.; Song, F.; Wang, X.-L.; Wang, Y.-Z. Dendritic Crystallization and Morphology Control of Random Poly(p-dioxanone-co-butylene-co-succinate) Copolyesters. *Eur. Polym. J.* **2018**, *108*, 76–84. [CrossRef]
71. Lu, H.; Tong, H.; Gao, B.; Zhu, J.; Zhang, S. Photothermal and Robust Supramolecular Soft Material Crosslinked via Dinuclear Heterodentate Coordination. *Mater. Horiz.* **2025**, *12*, 3127–3143. [CrossRef]
72. Paszkiewicz, S.; Szymczyk, A.; Irska, I.; Pawlikowska, D.; Piesowicz, E. Synthesis, Structure, and Physical Properties of Poly(trimethylene terephthalate)-Block-Poly(caprolactone) Copolymers. *J. Appl. Polym. Sci.* **2019**, *136*, 47341. [CrossRef]
73. Terzopoulou, Z.; Papadopoulos, L.; Zamboulis, A.; Papageorgiou, D.G.; Papageorgiou, G.Z.; Bikiaris, D.N. Tuning the Properties of Furandicarboxylic Acid-Based Polyesters with Copolymerization: A Review. *Polymers* **2020**, *12*, 1209. [CrossRef] [PubMed]
74. Wang, G.; Jiang, M.; Zhang, Q.; Wang, R.; Zhou, G. Biobased Multiblock Copolymers: Synthesis, Properties and Shape Memory Performance of Poly(ethylene 2,5-furandicarboxylate)-b-Poly(ethylene glycol). *Polym. Degrad. Stab.* **2017**, *144*, 121–127. [CrossRef]
75. Hu, H.; Zhang, R.; Kong, Z.; Wang, K.; Ying, W.B.; Wang, J.; Zhu, J. Bio-Based Poly(butylene furandicarboxylate)-b-Poly(ethylene glycol) Copolymers: The Effect of Poly(ethylene glycol) Molecular Weight on Thermal Properties and Hydrolysis Degradation Behavior. *Adv. Ind. Eng. Polym. Res.* **2019**, *2*, 167–177. [CrossRef]
76. Bianchi, E.; Soccio, M.; Siracusa, V.; Gazzano, M.; Thiyagarajan, S.; Lotti, N. Poly(butylene 2,4-furanoate), an Added Member to the Class of Smart Furan-Based Polyesters for Sustainable Packaging: Structural Isomerism as a Key to Tune the Final Properties. *ACS Sustain. Chem. Eng.* **2021**, *9*, 11937–11949. [CrossRef]
77. Poulopoulou, N.; Guigo, N.; Sbirrazzuoli, N.; Papageorgiou, D.G.; Bikiaris, D.N.; Nikolaidis, G.N.; Papageorgiou, G.Z. Towards Increased Sustainability for Aromatic Polyesters: Poly(butylene 2,5-furandicarboxylate) and Its Blends with Poly(butylene terephthalate). *Polymer* **2021**, *212*, 123157. [CrossRef]

78. Walkowiak, K.; Paszkiewicz, S.; Irska, I.; Kochmanska, A.; Dydek, K.; Boczkowska, A.; Stanik, R.; Gude, M.; Linares, A.; Ezquerra, T. Furan-Based Bionanocomposites Reinforced with a Hybrid System of Carbon Nanofillers. *Adv. Eng. Mater.* **2023**, *25*, 2300046. [CrossRef]
79. Walkowiak, K.; Paszkiewicz, S. Modifications of Furan-Based Polyesters with the Use of Rigid Diols. *Polymers* **2024**, *16*, 2064. [CrossRef] [PubMed]
80. Deng, Z.; Liubchak, I.; Holness, F.B.; Shahrokhi, F.; Price, A.D.; Gillies, E.R. Biobased Composites of Poly(butylene furanoate) Copolymers and Hemp. *J. Polym. Sci.* **2023**, *61*, 1528–1536. [CrossRef]
81. Paszkiewicz, S.; Walkowiak, K.; Barczewski, M. Biobased Polymer Nanocomposites Prepared by in Situ Polymerization: Comparison between Carbon and Mineral Nanofillers. *J. Mater. Sci.* **2024**, *59*, 13805–13823. [CrossRef]
82. Wunderlich, B. *Thermal Analysis of Polymeric Materials*; Springer: Berlin/Heidelberg, Germany, 2005.
83. Heidrich, D.; Gehde, M. The 3-Phase Structure of Polyesters (PBT, PET) after Isothermal and Non-Isothermal Crystallization. *Polymers* **2022**, *14*, 793. [CrossRef]
84. Guskos, N.; Typek, J.; Padlyak, B.V.; Gorelenko, Y.K.; Pelech, I.; Narkiewicz, U.; Piesowicz, E.; Guskos, A.; Roslaniec, Z. In Situ Synthesis, Morphology and Magnetic Properties of Poly(ether–ester) Multiblock Copolymer/Carbon-Covered Nickel Nanosystems. *J. Non-Cryst. Solids* **2010**, *356*, 1893–1901. [CrossRef]
85. Tereshatov, V.; Vnutskikh, Z.; Slobodinyuk, A.; Makarova, M.; Senichev, V. New Multi-Block Isophorone Diisocyanate-Based Copolymers with Urethane Urea Hard Segments. *J. Elastomers Plast.* **2016**, *48*, 289–304. [CrossRef]
86. Rosłaniec, Z. Dynamic Mechanical and Microcalorimetric Studies on the Phase Structure in Blends of Two Multiblock Copolymers: 1. Poly(ether-ester) and Poly((ether-carbonate)-urethane) Blends. *Polymer* **1993**, *34*, 1249–1255. [CrossRef]
87. Stevenson, J.C.; Cooper, S.L. Microstructure and Property Changes Accompanying Hard-Segment Crystallization in Block Copoly(ether-ester) Elastomers. *Macromolecules* **1988**, *21*, 1309–1316. [CrossRef]
88. Ukielski, R.; Lembicz, F. Effect of Chemical Modification of Poly(butylene terephthalate) on Elastic Properties. *Int. Polym. Sci. Technol.* **2004**, *31*, 70–75. [CrossRef]
89. Gavrilov, A.A.; Chertovich, A.V.; Khalatur, P.G.; Khokhlov, A.R. Study of the Mechanisms of Filler Reinforcement in Elastomer Nanocomposites. *Macromolecules* **2014**, *47*, 5400–5408. [CrossRef]
90. Barczewski, M.; Aniśko, J.; Piasecki, A.; Biedrzycka, K.; Moraczewski, K.; Stepczyńska, M.; Kloziński, A.; Szostak, M.; Hahn, J. The Accelerated Aging Impact on Polyurea Spray-Coated Composites Filled with Basalt Fibers, Basalt Powder, and Halloysite Nanoclay. *Compos. B Eng.* **2021**, *225*, 109286. [CrossRef]
91. Galeski, A. Strength and Toughness of Crystalline Polymer Systems. *Prog. Polym. Sci.* **2003**, *28*, 1643–1699. [CrossRef]
92. Brostow, W.; Hagg Lobland, H.E.; Khoja, S. Brittleness and Toughness of Polymers and Other Materials. *Mater. Lett.* **2015**, *159*, 478–480. [CrossRef]
93. Karger-Kocsis, J.; Kalló, A.; Szafner, A.; Bodor, G.; Sényei, Z. Morphological Study on the Effect of Elastomeric Impact Modifiers in Polypropylene Systems. *Polymer* **1979**, *20*, 37–43. [CrossRef]
94. Szymczyk, A.; Paszkiewicz, S.; Roslaniec, Z. Influence of Intercalated Organoclay on the Phase Structure and Physical Properties of PTT-PTMO Block Copolymers. *Polym. Bull.* **2013**, *70*, 1575–1590. [CrossRef]
95. Barczewski, M.; Lewandowski, K.; Rybarczyk, D.; Kloziński, A. Rheological and Single Screw Extrusion Processability Studies of Isotactic Polypropylene Composites Filled with Basalt Powder. *Polym. Test.* **2020**, *91*, 106768. [CrossRef]
96. de Lima Ferreira, I.M.; de Araújo, N.K.C.; de Melo Queiroz, G.S.; de Medeiros Batista, A.C.; de Melo Viana, G.A.C.; de Carvalho Galvão, L.P.F.; de Morais Araujo, A.M.; Gondim, A.D. Study of Thermal Decomposition of Microalgae Biomass Pretreated by Acetylation for Biofuel Production. *J. Therm. Anal. Calorim.* **2023**, *148*, 11825–11833. [CrossRef]
97. Han, C.D.; Chuang, H. Criteria for Rheological Compatibility of Polymer Blends. *J. Appl. Polym. Sci.* **1985**, *30*, 4431–4454. [CrossRef]
98. Chuang, H.; Han, C.D. Rheological Behavior of Polymer Blends. *J. Appl. Polym. Sci.* **1984**, *29*, 2205–2229. [CrossRef]
99. Balkan, O.; Ezdeşir, A. Rheological Behaviors of Glass Bead- and Wollastonite-filled Polypropylene Composites Modified with Thermoplastic Elastomers. *Polym. Compos.* **2012**, *33*, 1162–1187. [CrossRef]
100. Zhou, K.; Gu, S.; Zhang, Y.; Ren, J. Effect of Dispersion on Rheological and Mechanical Properties of Polypropylene/Carbon Nanotubes Nanocomposites. *Polym. Eng. Sci.* **2012**, *52*, 1485–1494. [CrossRef]
101. Vitiello, L.; Salzano de Luna, M.; Ambrogi, V.; Filippone, G. A Simple Rheological Method for the Experimental Assessment of the Fiber Percolation Threshold in Short Fiber Biocomposites. *Compos. Sci. Technol.* **2024**, *245*, 110345. [CrossRef]
102. Bhagat, A.B.; Ghosh, A.K. Estimation of Rheological Percolation Threshold and Influence of Fibre Length on Properties of Polypropylene/Sisal Fibre Composites Having near Critical Fibre Length. *Polymer* **2022**, *258*, 125304. [CrossRef]